

Mini-Batch Covariance, Diffusion Limits, and Oracle Complexity in Stochastic Gradient Descent: A Sampling-Design Perspective

Daniel Zantedeschi¹ and Kumar Muthuraman²

¹Muma College of Business, University of South Florida, Tampa, FL, USA,
danielz@usf.edu

²McCombs School of Business, University of Texas at Austin, Austin, TX, USA,
kumar.muthuraman@mcombs.utexas.edu

April 16, 2026

Abstract

Stochastic gradient descent (SGD) is central to simulation optimization, stochastic programming, and online M-estimation, where sampling effort is a decision variable. We study the mini-batch gradient noise as a sampling-design object. Under exchangeable fresh-sampling mini-batches, the conditional covariance given the de Finetti directing measure μ is $b^{-1}G_\mu(\theta)$, and under identifiability the projected population object is $b^{-1}G^*(\theta)$ —projected Fisher information for correctly specified likelihoods, the sandwich partner of the Hessian otherwise. This identification fixes the noise matrix entering the diffusion analysis of constant-step SGD: the raw iterate path has a deterministic fluid limit, and the $\sqrt{b/\eta}$ -scaled fluctuations satisfy a functional CLT with noise covariance G^* ; near a nondegenerate optimum the limit is Ornstein–Uhlenbeck, and its Lyapunov covariance scaled by η/b matches the linearized discrete recursion at leading order. Under a curvature–noise compatibility condition $\mu_F > 0$, we prove $1/N$ mean-square upper bounds and an i.i.d. parametric Fisher van Trees lower bound of the same rate order, with oracle-complexity guarantees depending on an effective dimension d_{eff} and condition number κ_F . Numerical experiments verify the identification and confirm the Lyapunov predictions in direct SGD.

Keywords: Stochastic gradient descent; simulation optimization; sampling-design; mini-batch covariance; diffusion limits; Ornstein–Uhlenbeck approximation; Fisher and Godambe information; oracle complexity; batch-size control

1 Introduction

Stochastic gradient descent (SGD) is the computational workhorse behind a large class of operations research and management science problems, including simulation optimization, large-scale stochastic programming, and data-driven estimation in service and supply-chain systems. In these settings, *sampling effort is a decision variable*: each iterate trades off additional replications (or scenarios) against the number of updates that can be executed under a fixed budget. Several widely observed phenomena depend on this trade-off: small mini-batches often dominate large batches in wall-clock efficiency; constant-step SGD exhibits steady-state “error floors” and implicit regularization; and the linearized local equilibrium of plain SGD exhibits directional structure related to the local curvature–noise geometry, despite the drift being unpreconditioned.

Classical stochastic approximation and diffusion-approximation analyses—small-step SDE surrogates, Ornstein–Uhlenbeck linearization, Lyapunov stationary covariance, \sqrt{t} -CLT scaling—are well-developed OR tools for analyzing such recursions once the gradient-noise covariance is specified (Kushner and Yin, 2003; Harrison, 1985; Whitt, 2002). We do not reprove that machinery. Our contribution is a sampling-design reinterpretation of the noise input: under exchangeable fresh-sampling mini-batches, the conditional mini-batch covariance is determined by the sampling mechanism at b^{-1} times the per-sample gradient covariance, a statement that is elementary but carries structural consequences for operational decisions about sampling budgets. Writing the identified matrix as $G^*(\theta)$ —projected Fisher information at the correctly specified point, and more generally the sandwich partner of the Hessian H^* —lets us analyze constant-step SGD in a fixed statistical metric rather than a Euclidean one, with the diffusion coefficient determined by the sampling design rather than postulated. Under a curvature–noise compatibility condition $\mu_F > 0$ (Assumption 6.2; not implied by $H^*, F^* \succ 0$ alone), the resulting local rates in the Fisher case match an i.i.d. van Trees lower bound in rate order, and batch size becomes a statistical design variable subject to a sampling budget.

1.1 Motivation: Simulation Optimization as Sampling Control

Consider the canonical simulation-optimization objective

$$\min_{\theta \in \Theta} L(\theta) := \mathbb{E}[h(\theta, \xi)], \tag{1}$$

where ξ denotes random inputs (arrivals, service times, demand shocks) and $h(\theta, \xi)$ is the induced cost. A standard stochastic-gradient estimator uses b simulation replications,

$$g_B(\theta) = \frac{1}{b} \sum_{i=1}^b \nabla_{\theta} h(\theta, \xi_i), \quad \xi_i \stackrel{\text{i.i.d.}}{\sim} P, \tag{2}$$

followed by $\theta^+ = \theta - \eta g_B(\theta)$. Classical variance-reduction intuition focuses on the scalar variance of a component or of a scalarized performance measure, suggesting that larger b should always help. In practice, under fixed sampling budgets, small b often wins.

The key reason is geometric: the noise in $g_B(\theta)$ is not scalar but a *matrix*-valued covariance that encodes which directions are intrinsically informative and which are weakly identified by the underlying experiment. The same sampling-control perspective applies to three canonical MOR problem classes: (i) *simulation optimization* (queuing, inventory, revenue management), where each mini-batch gradient requires b simulation replications and the replication budget is the binding constraint; (ii) *stochastic programming and SAA*, where scenario-based gradient estimates are drawn from an empirical distribution and the number of scenarios per iterate is a design variable subject to a total scenario budget; and (iii) *online M -estimation in service systems*, where per-transaction loss gradients arrive in a stream and the batch window trades off estimation quality against decision latency. In each case, sampling effort is explicit, b is typically small relative to d , and the question “how many samples per iterate?” is operationally binding.

1.2 Contributions and scope

Under exchangeable fresh-sampling mini-batches, the conditional mini-batch covariance given the de Finetti directing measure μ is $\text{Cov}(g_B(\theta) \mid \mu) = b^{-1}G_\mu(\theta)$ (Theorem 4.3). Under identifiability with a single data-generating distribution, the unconditional covariance reads

$$\text{Cov}(g_B(\theta)) = \frac{1}{b} G(\theta), \quad (3)$$

and, after projection onto the identifiable tangent space, we denote the resulting population object $G^*(\theta) := \Pi_\theta G(\theta) \Pi_\theta^\top$ (Section 4). All downstream results are stated in terms of G^* . For correctly specified likelihood losses, $G^*(\theta^*) = F^*(\theta^*)$; the finite-dataset-reuse case adds a $(1 - b/n)$ correction and is treated separately (Lemma 4.1, Proposition 4.5).

Once $G^*(\theta)$ is identified, three consequences follow within the classical stochastic-approximation toolkit. (a) At fixed batch size, constant-step SGD has a deterministic fluid limit (the gradient-flow ODE), and its $\sqrt{b/\eta}$ -scaled fluctuations obey a functional CLT converging to a linear SDE with noise covariance G^* ; near a nondegenerate optimum this is an OU process, and its stationary covariance, multiplied back by η/b , is the discrete-time Lyapunov benchmark of Proposition 5.13 (Section 5). (b) Mean-square error in the Fisher/identified metric admits a $1/N$ upper bound with an intrinsic effective dimension d_{eff} and statistical condition number κ_F (Section 6), matched in *rate order* by an i.i.d. parametric Fisher van Trees lower bound (Proposition 6.8); geometry dependence appears only in the upper bound. (c) A high-probability oracle-complexity statement follows, with a squared-gradient stationarity rate of order $N^{-1/2}$ (Theorem 7.3).

Main Results (informal).

Theorem 4.3 — Covariance identification under exchangeable fresh sampling: $\text{Cov}(g_B \mid \mu) = b^{-1}G_\mu(\theta)$; under identifiability and after projection onto the identifiable tangent space, the population covariance is $\text{Cov}(g_B) = b^{-1}G^*(\theta)$.

Theorem 5.7 — Fluid limit for the raw iterates and functional CLT for $\sqrt{b/\eta}$ -scaled fluctuations, with noise covariance determined by G^* .

Thm. 5.10, Cor. 5.11 — OU equilibrium at θ^* on the fluctuation scale; linearized discrete-recursion stationary covariance on the original scale, $\Sigma_\eta^{\text{lin}} = (\eta/b)\Sigma_U + o(\eta/b)$ (Prop. 5.13).

Thm. 6.5, Prop. 6.8 — $1/(Tb)$ upper bound and rate-order-matching i.i.d. Fisher lower bound.

Theorem 7.3 — Squared-gradient stationarity at rate $N^{-1/2}$; norm stationarity at $N^{-1/4}$.

1.3 Organization

Section 2 reviews related work. Section 3 defines the oracle model and geometric objects. Section 4 derives the covariance identification from exchangeability. Section 5 builds the diffusion approximation, OU linearization, and discrete-time bridge. Section 6 proves an upper bound and a rate-order-matching i.i.d. Fisher lower bound, and Section 7 states oracle complexity. Section 8 provides numerical validation, and Section 9 discusses extensions and practical implications.

2 Literature Review and Positioning

We organize prior work along two axes: (i) whether the mini-batch noise covariance is *assumed* (exogenous) or *derived* from the sampling mechanism; and (ii) whether rates are stated in a Euclidean or in the identified statistical metric. Table 1 summarizes the resulting taxonomy.

Stochastic approximation and stationary covariance. Classical SA theory studies recursions $\theta_{t+1} = \theta_t - \eta_t\{h(\theta_t) + \xi_{t+1}\}$ and derives a \sqrt{t} -CLT whose asymptotic covariance is governed by a Lyapunov equation involving the Jacobian and a long-run noise covariance Γ (Robbins and Monro, 1951; Dvoretzky, 1956; Kushner and Yin, 2003; Polyak and Juditsky, 1992). This framework takes Γ as given; the OU linearization, Lyapunov balance, and $1/\sqrt{t}$ scaling are standard consequences. Our contribution is logically prior: we derive $\Gamma = G^*(\theta)/b$ from the mini-batch sampling design (Theorem 4.3), converting the SA machinery from a conditional analysis into a structural one.

Diffusion approximations for SGD. A substantial literature interprets constant-step SGD as a discretization of an SDE with temperature $\tau = \eta/b$ and various proposed diffusion matrices $\mathbf{C}(\theta)$ (Mandt et al., 2017; Li et al., 2017; Smith et al., 2021). In those works the diffusion covariance is either postulated, estimated from running iterates, or justified heuristically through moment matching. Our covariance identification removes this modeling degree of freedom. At fixed

batch size, we do not claim a nondegenerate diffusion limit of the raw iterate path—its martingale variation is of order η/b and vanishes—but we prove a fluid limit plus a functional CLT on the $\sqrt{b/\eta}$ -rescaled fluctuations, with noise covariance $C^*C^{*\top} = G^*$ (Theorem 5.7). The local OU regime and the Lyapunov balance then appear as the equilibrium specialization on the fluctuation scale, with $\tau = \eta/b$ recovered on the original iterate scale (Theorem 5.10, Corollary 5.11). This is the standard stochastic-approximation functional CLT architecture (Kushner and Yin, 2003) applied to the fresh-sampling covariance identified in Section 4, and is what fixes the noise input to the subsequent rate analysis.

Scaling regimes. Recent rigorous diffusion-limit work studies joint regimes where b grows with d (Paquette et al., 2025). Our analysis is complementary and closer to OR operating constraints: we keep d fixed and treat b as a design variable subject to a budget, with particular attention to the common regime $b \ll d$ where the *matrix* geometry of $G^*(\theta)$ controls transient behavior and risk.

Information geometry, natural gradients, and Fisher-shaped preconditioning. Information geometry treats Fisher information as a Riemannian metric and motivates natural-gradient updates $\theta_{t+1} = \theta_t - \eta F(\theta_t)^{-1} \nabla L(\theta_t)$ (Amari, 1998; Martens, 2020). Related methods—including stochastic gradient Fisher scoring (Ahn et al., 2012) and KFAC (Martens and Grosse, 2015)—inject or exploit Fisher geometry exogenously in the drift or preconditioner. Our contribution is distinct: even plain SGD, without any preconditioning, inherits the identified statistical geometry endogenously through its noise covariance under mini-batch sampling, changing the interpretation of diffusion strength, stationary risk, and batch-size tuning without requiring natural-gradient updates.

Minimax rates and information-theoretic limits. Classical oracle lower bounds are stated in Euclidean norms under smoothness and strong convexity (Nemirovski et al., 2009; Agarwal et al., 2012), which may not reflect the intrinsic difficulty of statistical objectives. We give an upper bound in the identified statistical metric that surfaces dependence on κ_F and d_{eff} (Theorem 6.5), and match its $1/N$ rate with an i.i.d. van Trees lower bound in the parametric Fisher setting (Proposition 6.8); the lower bound is at the level of rate order and does not certify the geometry dependence.

OR context: sampling budgets. In simulation optimization and stochastic programming, gradients are estimated from sampled scenarios and sampling cost is explicit (Fu, 2006; Shapiro et al., 2014; Chernoff, 1959). Because batching controls temperature $\tau = \eta/b$, it directly shapes diffusion amplitude and terminal risk; Section 9 outlines the resulting effort allocation problem.

Table 1: Positioning: primitives, contrasts, and where each appears in the paper.

Primitive	Status quo	This paper	Pointers
Mini-batch noise covariance	Exogenous / isotropic / heuristic Γ	Identified from sampling: $\text{Cov}(g_B) \propto b^{-1}G^*(\theta)$; Fisher is a special case	Sec. 4; Thm. 4.3
Continuous-time limit	Postulated SDE with ad hoc $\mathbf{C}(\theta)$	Fluid limit (ODE) for raw iterates; functional CLT for $\sqrt{b/\eta}$ -scaled fluctuations with diffusion $G^*(\theta)$	Sec. 5; Thm. 5.7
OU / Lyapunov equilibrium	Heuristic OU with ad hoc covariance	OU fluctuation limit at θ^* ; Lyapunov balance $H^*\Sigma_U + \Sigma_U H^{*\top} = G^*$ on fluctuation scale; linearized original-scale benchmark $\Sigma_\eta^{\text{lin}} = (\eta/b)\Sigma_U + o(\eta/b)$ (Prop. 5.13 / Cor. 5.11)	Sec. 5; Cor. 5.11
Metric for rates	Euclidean distance; κ_H dominates	Identified statistical metric is the natural risk	Sec. 6; Thm. 6.5
Lower bounds	Euclidean oracle lower bounds	Information-theoretic lower bound in Fisher metric (van Trees)	Sec. 6; Prop. 6.8
Dimension notion	Ambient d	Effective dimension d_{eff} induced by F^* / G^*	Sec. 6; Def. (40)
Oracle complexity	Euclidean stationarity; κ_H	Fisher-dual stationarity; κ_F and d_{eff}	Sec. 7; Thm. 7.3

Why small batches can work when $b \ll d$. The empirical preference for small batches (Keskar et al., 2017; Shallue et al., 2019; McCandlish et al., 2018) is explained by our framework: smaller b buys more contraction steps under fixed budgets, the identified covariance concentrates noise along statistically flat directions, and rates scale with $d_{\text{eff}} \ll d$.

3 Problem Setup and Preliminaries

This section fixes notation, specifies the stochastic-gradient oracle, and records the geometric objects that govern the diffusion approximation and the rate/complexity bounds. The perspective is *Mathematics of Operations Research*: we make the sampling design explicit, separate intrinsic noise geometry from finite-population correction, and state the local regularity conditions used

throughout.

3.1 Notation and macros used throughout

We work on a measurable space $(\mathcal{Z}, \mathcal{A})$. Vectors use the Euclidean inner product $\langle u, v \rangle = u^\top v$ and norm $\|u\|_2$. For a symmetric matrix A , $\|A\|_{\text{op}}$ denotes the operator norm and $\lambda_{\min}(A), \lambda_{\max}(A)$ its extreme eigenvalues.

3.2 Data model, objective, and stochastic-gradient oracle

Let $\Theta \subseteq \mathbb{R}^d$ be open and convex. Let Q denote the (unknown) data distribution on $(\mathcal{Z}, \mathcal{A})$, and let $\ell : \Theta \times \mathcal{Z} \rightarrow \mathbb{R}$ be a measurable loss. Define the population risk

$$L(\theta) := \mathbb{E}_{Z \sim Q}[\ell(\theta; Z)], \quad (4)$$

and let $\theta^* \in \arg \min_{\theta \in \Theta} L(\theta)$ be a (local) minimizer.

Finite-population sampling model. We observe a dataset $z_{1:n} := (z_1, \dots, z_n)$ drawn i.i.d. from Q (or, in the exchangeability formulation of Section 4, conditionally i.i.d. given a directing measure). The lower bound in Section 6 is stated for the i.i.d. parametric Fisher setting; adaptive-oracle extensions are discussed in Remark 6.11. At iteration t , the algorithm selects a mini-batch $B_t \subseteq \{1, \dots, n\}$ of size b_t uniformly *without replacement* and forms the mini-batch gradient

$$g_t(\theta) := \frac{1}{b_t} \sum_{i \in B_t} \psi(\theta; z_i), \quad \psi(\theta; z) := \nabla_{\theta} \ell(\theta; z). \quad (5)$$

The SGD recursion is

$$\theta_{t+1} = \theta_t - \eta_t g_t(\theta_t), \quad (6)$$

with stepsize $\eta_t > 0$.

Filtration and martingale structure. Let \mathcal{F}_t be the σ -field generated by $(\theta_0, B_0, \dots, B_{t-1}, \theta_t)$ and the dataset $z_{1:n}$. Then

$$\xi_t(\theta_t) := g_t(\theta_t) - \mathbb{E}[g_t(\theta_t) \mid \mathcal{F}_t]$$

is a martingale difference sequence with respect to (\mathcal{F}_t) , and all diffusion limits are driven by the predictable quadratic variation of $\sum_t \eta_t \xi_t$.

Cost accounting (oracle calls). We measure computational cost in *sample-gradient evaluations*. One iteration with batch size b_t uses b_t sample evaluations. After T iterations, the total

sampling budget is

$$N_T := \sum_{t=0}^{T-1} b_t. \quad (7)$$

We report results both in iterations T and in oracle calls N_T , since control/OR questions naturally optimize over batch allocation under a fixed N_T .

3.3 Likelihood losses: Fisher information and the induced metric

When $\ell(\theta; z) = -\log p_\theta(z)$ for a parametric family $\{P_\theta : \theta \in \Theta\}$ with density p_θ , the score is $s_\theta(z) := \nabla_\theta \log p_\theta(z)$ and the loss gradient is the negative score, $\nabla_\theta \ell(\theta; z) = -s_\theta(z)$. The intrinsic noise geometry reduces to Fisher information at the correctly specified point θ^* .

Definition 3.1 (Fisher information). Assume p_θ is differentiable in θ and $s_\theta(Z)$ is square integrable under P_θ . The Fisher information is

$$F(\theta) := \mathbb{E}_\theta[s_\theta(Z)s_\theta(Z)^\top]. \quad (8)$$

Lemma 3.2 (Score identities (Lehmann and Casella, 1998, Ch. 7)). Assume $\int p_\theta(z) dz = 1$ and differentiation under the integral is valid. Then (i) $\mathbb{E}_\theta[s_\theta(Z)] = 0$ and (ii)

$$F(\theta) = -\mathbb{E}_\theta[\nabla_\theta^2 \log p_\theta(Z)]. \quad (9)$$

Proof. Standard; see, e.g., Lehmann and Casella (1998, Ch. 7). □

Fisher metric. If $F(\theta) \succ 0$, it defines the local inner product $\langle u, v \rangle_{F(\theta)} := u^\top F(\theta)v$ and norm $\|u\|_{F(\theta)} := \sqrt{u^\top F(\theta)u}$. On compact sets where $F(\theta)$ is bounded and bounded away from 0, Fisher and Euclidean norms are equivalent.

3.4 General losses: sandwich / Godambe geometry

For a general loss, information equality need not hold. The relevant local geometry splits into (i) curvature of the drift and (ii) covariance of the estimating equation (gradient).

Definition 3.3 (Noise covariance, sensitivity, and Godambe information). Let $\psi(\theta; z) := \nabla_\theta \ell(\theta; z)$ and define

$$G(\theta) := \text{Cov}(\psi(\theta; Z)), \quad (10)$$

$$H(\theta) := \nabla^2 L(\theta) = \mathbb{E}[\nabla_\theta \psi(\theta; Z)], \quad (11)$$

where expectations are under $Z \sim Q$. When $H(\theta)$ is invertible on the identifiable directions, the classical sandwich covariance and Godambe information are

$$\Sigma_{\text{sand}}(\theta) := H(\theta)^{-1}G(\theta)H(\theta)^{-1}, \quad J_{\text{God}}(\theta) := \Sigma_{\text{sand}}(\theta)^{-1} = H(\theta)^{\top}G(\theta)^{-1}H(\theta). \quad (12)$$

Remark 3.4 (Likelihood as a special case). If $\ell(\theta; z) = -\log p_{\theta}(z)$ and the model is correctly specified, then $\psi = s_{\theta}$ and $G(\theta) = H(\theta) = F(\theta)$ at θ^* , so the sandwich collapses and the Godambe geometry equals Fisher.

3.5 Projection onto identifiable directions

Projection is only needed when the parametrization is redundant or when only a lower-dimensional tangent space is identifiable.

Definition 3.5 (Tangent-space projection and projected geometry). Let $T_{\theta} \subseteq \mathbb{R}^d$ denote the identifiable tangent space at θ (i.e., the linear span of directions along which the loss varies at first order; formally $T_{\theta} := \text{range}(H(\theta))$, or equivalently $\text{supp}(F(\theta))$ in the likelihood case), and let Π_{θ} be the Euclidean-orthogonal projector onto T_{θ} . Define the projected noise covariance

$$G^*(\theta) := \Pi_{\theta} G(\theta) \Pi_{\theta}^{\top}, \quad (13)$$

and, in the likelihood case, the projected Fisher information

$$F^*(\theta) := \Pi_{\theta} F(\theta) \Pi_{\theta}^{\top}. \quad (14)$$

When $T_{\theta} = \mathbb{R}^d$, $\Pi_{\theta} = I$ and $G^* = G$, $F^* = F$.

Remark 3.6 (Terminological convention). Throughout the paper, the identified noise matrix is $G^*(\theta)$ (the projected gradient covariance). In the correctly specified likelihood case, $G^*(\theta^*) = F^*(\theta^*)$ (projected Fisher information). For general losses, $G^*(\theta^*)$ is *not* itself the Godambe information; rather, paired with the Hessian H^* it induces the classical sandwich covariance $H^{*-1}G^*H^{*-1}$ and, by inversion, the Godambe information $J_{\text{God}} = H^{*\top}G^{*-1}H^*$. Every theorem statement holds with G^* in the general case and specializes to F^* under correct specification. When we write ‘‘Fisher metric’’ or ‘‘Fisher-dual norm,’’ the general-loss reader should substitute the corresponding object defined by G^* ; the paired Godambe/sandwich interpretation always requires H^* as well.

Remark 3.7 (What enters later sections). Sections 4–5 show that the mini-batch noise covariance is (up to a sampling-design factor) exactly $G^*(\theta)/b_t$ and reduces to $F^*(\theta)/b_t$ under correct specification. This is the only matrix that enters the diffusion coefficient and Lyapunov balance.

3.6 Local regularity conditions

All results are local near θ^* and use standard smoothness/moment and nondegeneracy conditions.

Assumption 3.8 (Smoothness and moments). The loss $\ell(\theta; z)$ is twice continuously differentiable in θ . There exist constants $M < \infty$ and $m_4 < \infty$ such that for all θ in a neighborhood \mathcal{N} of θ^* :

- (a) $\|\nabla_{\theta}^2 \ell(\theta; z)\|_{\text{op}} \leq M$ almost surely;
- (b) $\mathbb{E}[\|\psi(\theta; Z)\|_2^4] \leq m_4$.

Assumption 3.9 (Local stability). The population risk is locally strongly convex at θ^* :

$$H^* := \nabla^2 L(\theta^*) \succeq \mu I \quad \text{for some } \mu > 0. \quad (15)$$

Assumption 3.10 (Geometric nondegeneracy). The intrinsic noise geometry is positive definite on identifiable directions:

$$G^*(\theta^*) \succeq \lambda_{\min} I \quad \text{for some } \lambda_{\min} > 0. \quad (16)$$

(In the correctly specified likelihood case this is $F^*(\theta^*) \succ 0$.)

Remark 3.11 (Role of assumptions). Assumptions 3.8–3.10 provide Taylor/moment control, a locally stable equilibrium, and nondegeneracy of the diffusion coefficient, respectively.

3.7 Key geometric parameters (preview)

Several quantities derived from the local geometry at θ^* govern the rate and complexity results of Sections 6–7. We collect their definitions here so the reader can refer to them before encountering the formal theorems.

Definition 3.12 (Fisher-strong-convexity constant). Let $H^* := \nabla^2 L(\theta^*)$ and $F^* := F(\theta^*)$ (or $G^*(\theta^*)$ for general losses). Define

$$\mu_F := \lambda_{\min} \left(\frac{(F^*)^{1/2} H^* (F^*)^{-1/2} + (F^*)^{-1/2} H^* (F^*)^{1/2}}{2} \right). \quad (17)$$

Equivalently, μ_F is the smallest eigenvalue of the symmetrized curvature–information interaction $\text{Sym}((F^*)^{1/2} H^* (F^*)^{-1/2})$.

Definition 3.13 (Fisher condition number and effective dimension).

$$\kappa_F := \frac{\lambda_{\max}(F^*)}{\lambda_{\min}(F^*)}, \quad d_{\text{eff}}(F^*) := \frac{\text{Tr}(F^*)}{\lambda_{\max}(F^*)} \in (0, d]. \quad (18)$$

Table 2: Key notation. All quantities are evaluated locally at or near θ^* unless noted otherwise.

Symbol	Meaning
$L(\theta) = \mathbb{E}[\ell(\theta; Z)]$	Population risk (loss)
$\psi(\theta; z) = \nabla_{\theta} \ell(\theta; z)$	Per-sample estimating equation (gradient)
$g_B(\theta)$	Mini-batch gradient estimator
$G(\theta) = \text{Cov}(\psi(\theta; Z))$	Gradient covariance; $G^* = \Pi G \Pi^{\top}$ projected
$F(\theta) = \mathbb{E}[s_{\theta} s_{\theta}^{\top}]$	Fisher information (likelihood case)
$F^*(\theta^*)$	Projected Fisher; equals $G^*(\theta^*)$ under correct specification
$H^* = \nabla^2 L(\theta^*)$	Hessian at optimum (drift curvature)
$J_{\text{God}} = H^{\top} G^{-1} H$	Godambe (sandwich) information
$\tau = \eta/b$	Effective temperature
μ_F	Fisher-strong-convexity constant (Def. 3.12)
κ_F	Fisher condition number (Def. 3.13)
$d_{\text{eff}}(F^*)$	Effective dimension / stable rank of F^*

The quantity κ_F measures statistical anisotropy rather than Euclidean ill-conditioning; a problem can be Euclidean-stiff ($\kappa_H \gg 1$) yet statistically well-conditioned ($\kappa_F = O(1)$) when curvature and information share eigenstructure. The effective dimension d_{eff} is the stable rank of F^* : it equals d when F^* is isotropic and approaches 1 when a single direction dominates.

Remark 3.14 (Generalized eigenvalue interpretation). The constant μ_F is linked to the generalized eigenvalues of the pair (H^*, F^*) . If H^* and F^* commute (i.e., share an eigenbasis $\{v_j\}$ with respective eigenvalues h_j and f_j), then $(F^*)^{1/2} H^* (F^*)^{-1/2}$ has eigenvalues $f_j^{1/2} h_j f_j^{-1/2} = h_j$, so the symmetrization is trivial and $\mu_F = \min_j h_j = \lambda_{\min}(H^*)$: the Fisher-strong-convexity constant reduces to the ordinary strong-convexity constant. In the non-commuting case, $(F^*)^{1/2} H^* (F^*)^{-1/2}$ is non-normal (its eigenvalues are still those of H^* , but it is no longer symmetric), and the minimum of its quadratic form—i.e., μ_F —can drop strictly below $\lambda_{\min}(H^*)$. Geometrically, this occurs when the Fisher metric amplifies directions along which curvature is weak, making the effective contraction rate slower than the Euclidean strong-convexity constant. The product $\kappa_F \cdot d_{\text{eff}}$ that enters the oracle complexity (Theorem 7.3) therefore measures the total cost of resolving all statistically relevant directions at the hardest direction’s scale.

4 Covariance Identification for Mini-Batch Noise

Mini-batch gradient noise is not an arbitrary covariance: it is determined by (i) the sampling design used to form mini-batches and (ii) the intrinsic covariance of the per-sample estimating equation $\psi(\theta; Z)$ (Fisher information in the well-specified likelihood case, the projected gradient covariance more generally). We make this precise in two steps:

- an *exact* finite-population identity conditional on the realized dataset (classical survey-sampling algebra), and
- an *exchangeable/i.i.d.* limit that converts the dataset-dependent quantity into the population covariance $G(\theta) := \text{Cov}(\psi(\theta; Z))$ (or its projected analogue).

4.1 Finite-population covariance identity (exact, conditional on data)

Fix θ and condition on the realized dataset $\{z_1, \dots, z_n\}$. Write $\psi_i := \psi(\theta; z_i)$ and define the finite-population mean and covariance

$$\bar{\psi}_n(\theta) := \frac{1}{n} \sum_{i=1}^n \psi_i, \quad S_n(\theta) := \frac{1}{n-1} \sum_{i=1}^n (\psi_i - \bar{\psi}_n)(\psi_i - \bar{\psi}_n)^\top.$$

Let B be a simple random sample without replacement of size b from $\{1, \dots, n\}$ and define the mini-batch average

$$g_B(\theta) := \frac{1}{b} \sum_{i \in B} \psi_i.$$

Lemma 4.1 (Exact finite-population covariance of the mini-batch mean). *Conditionally on the dataset,*

$$\text{Cov}(g_B(\theta) \mid z_{1:n}) = \frac{1}{b} \left(1 - \frac{b}{n}\right) S_n(\theta). \quad (19)$$

Proof. Write $g_B(\theta) = \frac{1}{b} \sum_{i=1}^n I_i \psi_i$ where $I_i = \mathbf{1}\{i \in B\}$. Under simple random sampling without replacement, $\mathbb{E}[I_i] = b/n$, $\text{Var}(I_i) = \frac{b}{n}(1 - \frac{b}{n})$, and for $i \neq j$, $\text{Cov}(I_i, I_j) = -\frac{b(n-b)}{n^2(n-1)}$. Expanding $\text{Cov}(\sum_i I_i \psi_i \mid z_{1:n})$ and collecting terms yields (19). \square

Remark 4.2 (Equivalent correction-factor forms). Using S_n with the $1/(n-1)$ normalization gives the factor $(1 - b/n)$. If instead one uses the $1/n$ covariance normalization, the factor becomes $1 - (b-1)/(n-1)$. The two are algebraically equivalent up to the change of normalization.

Lemma 4.1 is the clean MOR-style decomposition: *sampling design* contributes the scalar finite-population correction $1 - b/n$, while the *geometry* lives in $S_n(\theta)$.

4.2 From exchangeability to the population covariance

We now convert the dataset-dependent covariance $S_n(\theta)$ into a population-level object.

Let $(Z_i)_{i \geq 1}$ be exchangeable with de Finetti directing measure μ (Hewitt and Savage, 1955). Conditional on μ , the sequence is i.i.d. with law P_μ . Define the population covariance (conditional on μ)

$$G_\mu(\theta) := \text{Cov}_\mu(\psi(\theta; Z)), \quad Z \sim P_\mu, \quad (20)$$

and, when identifiability requires it, the projected version $G_\mu^*(\theta) := \Pi_\theta G_\mu(\theta) \Pi_\theta^\top$.

Theorem 4.3 (Covariance identification under exchangeability). *Assume $\mathbb{E}_\mu \|\psi(\theta; Z)\|_2^2 < \infty$. Let $g_B(\theta) = \frac{1}{b} \sum_{i \in B} \psi(\theta; Z_i)$ where B is a uniform subset of $\{1, \dots, n\}$ of size b (sampling without replacement). Then, conditional on μ ,*

$$\text{Cov}(g_B(\theta) \mid \mu) = \frac{1}{b} G_\mu(\theta). \quad (21)$$

When the conditional mean $\mathbb{E}[\psi(\theta; Z) \mid \mu]$ does not vary with μ (identifiability under a single data-generating distribution), the unconditional covariance reads $\text{Cov}(g_B(\theta)) = b^{-1}G(\theta)$ where $G(\theta) := \mathbb{E}_\mu[G_\mu(\theta)]$; after projection onto the identifiable tangent space (Section 3), we denote this $G^*(\theta) = \Pi_\theta G(\theta) \Pi_\theta^\top$. The remainder of the paper works with G^* . Interpretation. Equation (21) is exact (not an approximation) when one marginalizes over both the mini-batch index B and the dataset realization conditional on μ . The finite-population correction $(1-b/n)$ of Lemma 4.1 is present when one conditions on a fixed dataset, but it disappears at the population level because the randomness of the dataset itself contributes a complementary term through the total-covariance decomposition. Equation (22) below makes this bookkeeping explicit.

Moreover,

$$\mathbb{E}[\text{Cov}(g_B(\theta) \mid Z_{1:n}, \mu) \mid \mu] = \frac{1}{b} \left(1 - \frac{b}{n}\right) \mathbb{E}[S_n(\theta) \mid \mu] = \frac{1}{b} \left(1 - \frac{b}{n}\right) G_\mu(\theta), \quad (22)$$

and the remaining part of (21) comes from the randomness of the dataset through the total-covariance decomposition.

Proof. Conditional on μ , the sequence $(Z_i)_{i \geq 1}$ is i.i.d. with law P_μ ; therefore any uniformly sampled subset of size b has the same joint distribution as the first b coordinates. Hence selecting indices B without replacement from $\{1, \dots, n\}$ is distributionally equivalent to taking the first b terms, and $g_B(\theta)$ is the average of b i.i.d. draws from P_μ . This yields $\text{Cov}(g_B(\theta) \mid \mu) = \frac{1}{b} G_\mu(\theta)$, proving (21).

For (22), apply the exact identity Lemma 4.1 conditional on $(Z_{1:n}, \mu)$ and take $\mathbb{E}[\cdot \mid \mu]$. Under $\mathbb{E}_\mu \|\psi\|^2 < \infty$, $\mathbb{E}[S_n(\theta) \mid \mu] = G_\mu(\theta)$ (the $1/(n-1)$ sample-covariance normalization is unbiased). \square

Remark 4.4 (What “alignment” means operationally). Equation (21) is the alignment statement used by the diffusion/Lyapunov analysis: *mini-batch noise has covariance $\frac{1}{b}$ times a population matrix determined by the loss and the data law.* The finite-population correction in Lemma 4.1 matters when one conditions on a fixed dataset and reuses it many times; in the standard stochastic-approximation regime with fresh randomness across iterations, the population covariance (21) is the relevant object.

Proposition 4.5 (Finite-population correction under dataset reuse). *Under the notation of Theorem 4.3, three conditioning levels yield distinct covariance expressions:*

- (i) Conditional on the dataset $z_{1:n}$ (fixed pool, sampling without replacement): $\text{Cov}(g_B(\theta) \mid z_{1:n}) = \frac{1}{b} \left(1 - \frac{b}{n}\right) S_n(\theta)$ (Lemma 4.1).

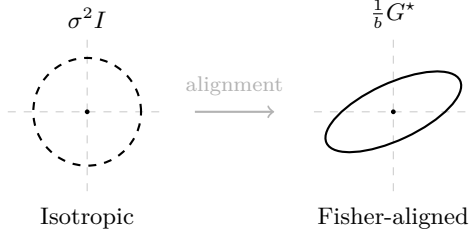


Figure 1: Isotropic noise (left, dashed circle) vs. Fisher-aligned noise (right, solid ellipse) at the same total variance. Batch size rescales temperature but not shape.

- (ii) Conditional on the directing measure μ (fresh data per iteration): $\text{Cov}(g_B(\theta) \mid \mu) = \frac{1}{b} G_\mu(\theta)$ (Theorem 4.3), with no finite-population correction.
- (iii) Population level (unconditional): $\text{Cov}(g_B(\theta)) = \frac{1}{b} \mathbb{E}_\mu[G_\mu(\theta)] + \text{Cov}_\mu(\mathbb{E}[g_B(\theta) \mid \mu])$. This reduces to $\frac{1}{b} G(\theta)$ when the conditional mean $\mathbb{E}[\psi(\theta; Z) \mid \mu]$ does not vary with μ (e.g., under identifiability with a single data-generating distribution).

When a finite dataset is reused across many iterations (i.e., without-replacement sampling from the same $z_{1:n}$ at every step), the conditional covariance carries the factor $(1 - b/n)$, which is non-negligible unless $b = o(n)$. The main diffusion, rate, and complexity results (Sections 5–7) are population-level or fresh-sampling statements that use level (ii).

Proof. Level (i) is Lemma 4.1. Level (ii) is Theorem 4.3. Level (iii) follows by integrating level (ii) over μ under identifiability. The total-covariance decomposition $\text{Cov}(g_B) = \mathbb{E}_\mu[\text{Cov}(g_B \mid \mu)] + \text{Cov}_\mu(\mathbb{E}[g_B \mid \mu])$ reconciles levels (ii) and (iii), with the second term contributing when $\mathbb{E}[g_B \mid \mu]$ varies with μ . \square

Remark 4.6 (Batch size rescales temperature, not geometry). Equation (21) implies that increasing the batch size b rescales the effective temperature $\tau = \eta/b$ (Section 5) but does *not* alter the noise ellipsoid: its shape is entirely determined by the statistical geometry $G_\mu(\theta)$. This decoupling—scale from the sampling budget, shape from the loss—underlies the subsequent rate and complexity results.

Remark 4.7 (Specialization to Fisher alignment). If $\ell(\theta; z) = -\log p_\theta(z)$ and the model is correctly specified, then $\psi(\theta; z) = s_\theta(z)$ is the score and the Bartlett identity yields $\text{Cov}(s_\theta(Z)) = F(\theta)$ at $\theta = \theta^*$. Projecting onto the identifiable tangent space gives $G_\mu^*(\theta^*) = F^*(\theta^*)$. Thus (21) becomes $\text{Cov}(g_B(\theta^*) \mid \mu) = \frac{1}{b} F^*(\theta^*)$, i.e., Fisher alignment.

Remark 4.8 (No Gaussian assumption). Neither Lemma 4.1 nor Theorem 4.3 assumes Gaussian noise. Gaussianity enters later only as a *diffusion approximation* (martingale CLT) when we pass from the discrete recursion to an OU limit.

5 Diffusion Limits: Fluid Scale, Fluctuation Scale, and the OU Regime

This section links the discrete-time SGD recursion to a continuous-time stochastic process whose diffusion coefficient is determined by the mini-batch covariance $G^*(\theta)$ identified in Section 4. The link is *not* a raw diffusion limit at fixed batch size: the martingale quadratic variation of the raw interpolation is of order η/b and vanishes as $\eta \downarrow 0$, so the raw process converges to the deterministic gradient-flow ODE. The nondegenerate stochastic limit appears only after centering around that ODE and rescaling by $\sqrt{b/\eta}$, yielding a fluctuation process whose limiting covariance structure is exactly G^* . Near a nondegenerate optimum, this fluctuation process is an Ornstein–Uhlenbeck (OU) process whose stationary covariance Σ_U satisfies a fluctuation-scale Lyapunov equation. On the original iterate scale, the linearized discrete recursion of Proposition 5.13 admits a unique stationary covariance Σ_η^{lin} that matches $(\eta/b)\Sigma_U$ at leading order in η , recovering the paper’s “effective temperature” $\tau = \eta/b$ on the correct scale; we do not claim an invariant law for the nonlinear SGD iterates. Diffusion approximations are a standard tool in OR for reducing stochastic systems to tractable Brownian models (Harrison, 1985; Whitt, 2002); the present setting is analogous, with the sampling mechanism playing the role of the arrival process.

Throughout this section we work in the *fresh-sampling / population* conditioning regime of Theorem 4.3: at each iterate the mini-batch is a simple random sample drawn with fresh randomness from the population (equivalently, conditional on the de Finetti directing measure μ). The fixed-dataset reuse case with $(1 - b/n)$ correction belongs to Lemma 4.1 and Proposition 4.5 and is not used below.

5.1 SGD recursion and the martingale-noise decomposition

Fix a batch size $b \in \mathbb{N}$ and a step size $\eta > 0$. Let

$$h(\theta) := \nabla L(\theta) = \mathbb{E}[\psi(\theta; Z)], \quad \psi(\theta; z) := \nabla_\theta \ell(\theta; z),$$

and write the mini-batch gradient estimator as $g_t(\theta_t) = h(\theta_t) + \xi_t(\theta_t)$ with $\mathbb{E}[\xi_t(\theta_t) \mid \mathcal{F}_t] = 0$, where \mathcal{F}_t is the natural filtration. The SGD recursion is

$$\theta_{k+1}^\eta = \theta_k^\eta - \eta h(\theta_k^\eta) - \eta \xi_{k+1}^\eta, \tag{23}$$

with the superscript η emphasizing the dependence of the iterate path on the step size. Under the fresh-sampling conditioning,

$$\mathbb{E}[\xi_{k+1}^\eta (\xi_{k+1}^\eta)^\top \mid \mathcal{F}_k^\eta] = \frac{1}{b} G^*(\theta_k^\eta) + r_{k+1}^\eta, \tag{24}$$

with remainder r_{k+1}^η satisfying the uniform bound stated in Assumption 5.2 below. We call $\tau := \eta/b$ the *effective temperature*:

$$\tau := \eta/b, \tag{25}$$

the scalar that sets the size of the stationary fluctuations on the original iterate scale (Corollary 5.11).

The covariance identification of Section 4 determines the noise geometry, but at fixed batch size b the raw interpolation of SGD on algorithmic time $t = k\eta$ has martingale quadratic variation of order η/b , which vanishes as $\eta \downarrow 0$. Accordingly, the raw process converges to the deterministic gradient-flow ODE. The correct nondegenerate stochastic limit is obtained by centering around that ODE and rescaling by $\sqrt{b/\eta}$, yielding a fluctuation process whose limiting covariance structure is exactly G^* .

5.2 Assumptions for the fluid and fluctuation limits

Assumption 5.1 (Local regularity and ODE flow). There is an open neighborhood $\mathcal{U} \subseteq \mathbb{R}^d$ such that:

- (i) $h \in C^1(\mathcal{U}; \mathbb{R}^d)$ and ∇h is locally Lipschitz on \mathcal{U} ;
- (ii) $G^* : \mathcal{U} \rightarrow \mathbb{S}_+^d$ is continuous;
- (iii) the ODE $\dot{\bar{\theta}}(t) = -h(\bar{\theta}(t))$ with $\bar{\theta}(0) = \theta_0$ has a unique solution on $[0, T]$ remaining in a compact set $K \Subset \mathcal{U}$.

Assumption 5.2 (Martingale noise and conditional covariance). The sequence $(\xi_{k+1}^\eta, \mathcal{F}_{k+1}^\eta)$ is a martingale difference, and the conditional covariance admits the expansion (24) with

$$\sup_{k \leq T/\eta} \|r_{k+1}^\eta\|_{\text{op}} \xrightarrow{\mathbb{P}} 0 \quad \text{as } \eta \downarrow 0.$$

Assumption 5.3 (Conditional fourth-moment bound on K). There is a constant $C_K < \infty$ such that

$$\sup_{\eta > 0} \sup_{k \leq T/\eta} \mathbb{E} \left[\|\xi_{k+1}^\eta\|^4 \mathbf{1}_{\{\theta_k^\eta \in K\}} \mid \mathcal{F}_k^\eta \right] \leq C_K \quad \text{a.s.}$$

Assumption 5.4 (Localization). $\Pr(\theta_k^\eta \in K \text{ for all } k \leq T/\eta) \rightarrow 1$ as $\eta \downarrow 0$.

Assumption 5.5 (Initial fluctuations converge). $\theta_0^\eta \rightarrow \theta_0$, and $U_0^\eta := \sqrt{b/\eta}(\theta_0^\eta - \theta_0) \Rightarrow U_0$ for some random variable U_0 .

Remark 5.6 (Verifiability). Assumptions 5.2–5.3 hold if $\sup_{\theta \in \mathcal{U}} \mathbb{E}[\|\psi(\theta; Z)\|^4] < \infty$ (guaranteed by Assumption 3.8(b)), G^* is continuous on \mathcal{U} , and the mini-batch is drawn by simple random sampling from an exchangeable sequence. Assumption 5.4 is standard in stochastic approximation

(Kushner–Yin style) and holds, e.g., when the ODE is globally stable and the initial iterate is in the basin.

5.3 Fluid limit and fluctuation theorem

Theorem 5.7 (Fluid limit and fluctuation limit at fixed batch size). *Fix $T > 0$ and $b \in \mathbb{N}$, and suppose Assumptions 5.1–5.5 hold. Let $\hat{\theta}^\eta(t) := \theta_{\lfloor t/\eta \rfloor}^\eta$ be the step interpolation of the SGD iterates (23), and let $\bar{\theta}$ solve the ODE in Assumption 5.1(iii). Then:*

(a) Fluid limit.

$$\sup_{t \in [0, T]} \|\hat{\theta}^\eta(t) - \bar{\theta}(t)\| \xrightarrow{\mathbb{P}} 0.$$

(b) Fluctuation FCLT. *The rescaled fluctuation process*

$$U^\eta(t) := \sqrt{\frac{b}{\eta}} (\hat{\theta}^\eta(t) - \bar{\theta}(t))$$

converges weakly in $D([0, T]; \mathbb{R}^d)$ (equivalently, in $C([0, T]; \mathbb{R}^d)$, as the limit is continuous) to the unique weak solution U of the linear SDE

$$dU_t = -\nabla h(\bar{\theta}(t)) U_t dt + C^*(\bar{\theta}(t)) dW_t, \quad U_0 \text{ as in Assumption 5.5,} \quad (26)$$

where W is a standard d -dimensional Brownian motion and $C^(\theta)C^*(\theta)^\top = G^*(\theta)$ (e.g., the symmetric PSD square root of G^*).*

Equivalently, on the original iterate scale,

$$\hat{\theta}^\eta(t) = \bar{\theta}(t) + \sqrt{\frac{\eta}{b}} U_t + o_{\mathbb{P}}\left(\sqrt{\frac{\eta}{b}}\right), \quad (27)$$

uniformly on $[0, T]$.

Proof. We follow the standard stochastic-approximation FCLT architecture (cf. Kushner and Yin, 2003, Ch. 8), tailored to the fresh-sampling covariance (24). Write $t_k := k\eta$ and $\bar{\theta}_k := \bar{\theta}(t_k)$; on the localization event of Assumption 5.4, which has probability tending to 1, the iterates stay in K for all $k \leq T/\eta$, and we work under this event without further comment.

Step 1 (fluid limit). Define the raw error $e_k^\eta := \theta_k^\eta - \bar{\theta}_k$ and the ODE local truncation error $\rho_{k+1}^\eta := \bar{\theta}_{k+1} - \bar{\theta}_k + \eta h(\bar{\theta}_k)$. Local Lipschitzness of h on K gives $\sup_{k \leq T/\eta} \|\rho_{k+1}^\eta\| \leq C_T \eta^2$ for some $C_T < \infty$. Subtracting the Euler step for $\bar{\theta}$ from (23),

$$e_{k+1}^\eta = e_k^\eta - \eta(h(\theta_k^\eta) - h(\bar{\theta}_k)) - \eta \xi_{k+1}^\eta - \rho_{k+1}^\eta. \quad (28)$$

Let $N_n^\eta := \eta \sum_{j=0}^{n-1} \xi_{j+1}^\eta$; this is an \mathcal{F}_k^η -martingale. Set $\bar{G}_K := \sup_{\theta \in K} \text{Tr} G^*(\theta) < \infty$ (finite by

continuity of G^* on the compact set K). By Doob's maximal inequality and Assumptions 5.2–5.3,

$$\mathbb{E}\left[\sup_{n \leq T/\eta} \|N_n^\eta\|^2\right] \leq 4\eta^2 \sum_{j < T/\eta} \mathbb{E}\|\xi_{j+1}^\eta\|^2 \leq 4\eta^2 \cdot \frac{T}{\eta} \cdot \frac{\bar{G}_K + o(1)}{b} = O(\eta/b).$$

Hence $\sup_{n \leq T/\eta} \|N_n^\eta\| \xrightarrow{\mathbb{P}} 0$. Using local Lipschitzness of h on K (constant L_K) in (28),

$$\|e_n^\eta\| \leq \|e_0^\eta\| + L_K \eta \sum_{j=0}^{n-1} \|e_j^\eta\| + \sup_{m \leq n} \|N_m^\eta\| + C_T T \eta,$$

and discrete Grönwall gives

$$\sup_{n \leq T/\eta} \|e_n^\eta\| \leq e^{L_K T} \left(\|e_0^\eta\| + \sup_{m \leq T/\eta} \|N_m^\eta\| + C_T T \eta \right) \xrightarrow{\mathbb{P}} 0,$$

since $\|e_0^\eta\| \rightarrow 0$ by Assumption 5.5. This establishes part (a).

Step 2 (rescaled recursion). Set $U_k^\eta := \sqrt{b/\eta} e_k^\eta$. Local Lipschitzness of ∇h on K gives the Taylor expansion $h(\theta_k^\eta) - h(\bar{\theta}_k) = A_k^\eta e_k^\eta + q_k^\eta$ with $A_k^\eta := \nabla h(\bar{\theta}_k)$ and $\|q_k^\eta\| \leq L'_K \|e_k^\eta\|^2$. Multiplying (28) by $\sqrt{b/\eta}$ and using $\eta\sqrt{b/\eta} = \sqrt{\eta b}$,

$$U_{k+1}^\eta = U_k^\eta - \eta A_k^\eta U_k^\eta + \Delta M_{k+1}^\eta + \varepsilon_{k+1}^\eta, \quad (29)$$

with

$$\Delta M_{k+1}^\eta := -\sqrt{\eta b} \xi_{k+1}^\eta, \quad \varepsilon_{k+1}^\eta := -\sqrt{\eta b} q_k^\eta - \sqrt{\frac{b}{\eta}} \rho_{k+1}^\eta. \quad (30)$$

Step 3 (tightness scale and remainders). From Step 1, $\sup_n \|e_n^\eta\| = e^{L_K T} (\|e_0^\eta\| + \sup \|N^\eta\| + C_T T \eta)$. Multiplying by $\sqrt{b/\eta}$,

$$\sup_n \|U_n^\eta\| \leq e^{L_K T} \left(\|U_0^\eta\| + \sqrt{\frac{b}{\eta}} \sup_m \|N_m^\eta\| + C_T T \sqrt{b\eta} \right).$$

The first term is tight by Assumption 5.5; $\mathbb{E}[(b/\eta) \sup_m \|N_m^\eta\|^2] \leq 4b/\eta \cdot O(\eta/b) = O(1)$, so the second is $O_{\mathbb{P}}(1)$; the third tends to 0. Hence

$$\sup_{n \leq T/\eta} \|U_n^\eta\| = O_{\mathbb{P}}(1). \quad (31)$$

Using (31) in the Taylor-remainder bound,

$$\left\| \sum_{k < n} \sqrt{\eta b} q_k^\eta \right\| \leq \sqrt{\eta b} \cdot L'_K \sum_{k < n} \|e_k^\eta\|^2 \leq L'_K T \sqrt{\frac{\eta}{b}} \sup_k \|U_k^\eta\|^2 \xrightarrow{\mathbb{P}} 0,$$

and, since $\|\rho_{k+1}^\eta\| \leq C_T \eta^2$,

$$\left\| \sum_{k < n} \sqrt{\frac{b}{\eta}} \rho_{k+1}^\eta \right\| \leq \frac{T}{\eta} C_T \eta^2 \sqrt{\frac{b}{\eta}} = C_T T \sqrt{b\eta} \rightarrow 0.$$

Hence $\sup_{t \leq T} \|\sum_{k < t/\eta} \varepsilon_{k+1}^\eta\| \xrightarrow{\mathbb{P}} 0$.

Step 4 (martingale FCLT). Let $M^\eta(t) := \sum_{k < t/\eta} \Delta M_{k+1}^\eta = -\sqrt{\eta b} \sum_{k < t/\eta} \xi_{k+1}^\eta$. By (24) its predictable quadratic variation is

$$\langle M^\eta \rangle(t) = \eta b \sum_{k < t/\eta} \mathbb{E}[\xi_{k+1}^\eta (\xi_{k+1}^\eta)^\top | \mathcal{F}_k^\eta] = \eta \sum_{k < t/\eta} G^*(\theta_k^\eta) + \eta b \sum_{k < t/\eta} r_{k+1}^\eta.$$

The remainder is bounded uniformly in $t \leq T$ by $Tb \cdot \sup_k \|r_{k+1}^\eta\| \xrightarrow{\mathbb{P}} 0$ under Assumption 5.2. For the leading term, continuity of G^* on K and the fluid limit $\sup_k \|\theta_k^\eta - \bar{\theta}_k\| \rightarrow 0$ (Step 1) give $\eta \sum_{k < t/\eta} \|G^*(\theta_k^\eta) - G^*(\bar{\theta}_k)\| \rightarrow 0$ in probability uniformly in t ; and $\eta \sum_{k < t/\eta} G^*(\bar{\theta}_k) \rightarrow \int_0^t G^*(\bar{\theta}(s)) ds$ is a Riemann-sum approximation with continuous integrand. Hence

$$\langle M^\eta \rangle(t) \Rightarrow \int_0^t G^*(\bar{\theta}(s)) ds \quad \text{uniformly on } [0, T].$$

For the conditional Lindeberg condition, using $\mathbf{1}_{\{x > \varepsilon\}} \leq x^2/\varepsilon^2$,

$$\sum_{k < T/\eta} \mathbb{E}[\|\Delta M_{k+1}^\eta\|^2 \mathbf{1}_{\{\|\Delta M_{k+1}^\eta\| > \varepsilon\}} | \mathcal{F}_k^\eta] \leq \frac{(\eta b)^2}{\varepsilon^2} \sum_{k < T/\eta} \mathbb{E}[\|\xi_{k+1}^\eta\|^4 | \mathcal{F}_k^\eta] \leq \frac{\eta b^2 T C_K}{\varepsilon^2} \rightarrow 0.$$

The martingale FCLT (Ethier and Kurtz, 1986, Theorem 7.1.4) then gives $M^\eta \Rightarrow M$ in $D([0, T]; \mathbb{R}^d)$, where M is a continuous Gaussian martingale with quadratic variation $\int_0^t G^*(\bar{\theta}(s)) ds$. Lévy's characterization yields a Brownian motion W with $M_t = \int_0^t C^*(\bar{\theta}(s)) dW_s$, and $C^*(\bar{\theta}(\cdot))$ can be taken as the (continuous) symmetric PSD square root of $G^*(\bar{\theta}(\cdot))$.

Step 5 (identify the limiting SDE). Summing (29) and using Step 3,

$$U^\eta(t) = U_0^\eta - \int_0^t \nabla h(\bar{\theta}(\lfloor s/\eta \rfloor \eta)) U^\eta(s) ds + M^\eta(t) + o_{\mathbb{P}}(1),$$

uniformly on $[0, T]$. Continuity of $s \mapsto \nabla h(\bar{\theta}(s))$ and tightness $\sup_t \|U^\eta(t)\| = O_{\mathbb{P}}(1)$ give $\int_0^t \nabla h(\bar{\theta}(\lfloor s/\eta \rfloor \eta)) U^\eta(s) ds - \int_0^t \nabla h(\bar{\theta}(s)) U^\eta(s) ds \rightarrow 0$ uniformly in probability. Tightness of $\{U^\eta\}$ in $D([0, T]; \mathbb{R}^d)$ follows from (31) and the controlled drift together with Aldous' criterion applied to the martingale term (whose FCLT is in hand). Any subsequential weak limit U therefore satisfies the stochastic integral equation

$$U_t = U_0 - \int_0^t \nabla h(\bar{\theta}(s)) U_s ds + \int_0^t C^*(\bar{\theta}(s)) dW_s,$$

which is (26) in integrated form. The linear SDE (26) with continuous coefficients admits a unique weak solution, so the entire sequence converges: $U^\eta \Rightarrow U$.

Step 6 (expansion). By construction $\hat{\theta}^\eta(t) - \bar{\theta}(t) = \sqrt{\eta/b} U^\eta(t)$; combining (a) and (b) gives (27). The asymptotic equivalence of step and piecewise-linear interpolations under Assumption 5.3 is standard and yields the same limit for either choice. \square

Remark 5.8 (Why the raw process is deterministic in the limit). At fixed b , the martingale variation of the raw interpolation is $\sum_{k < t/\eta} \eta^2 b^{-1} G^*(\theta_k^\eta) \sim (\eta/b) \int_0^t G^*(\bar{\theta}(s)) ds$, which vanishes as $\eta \downarrow 0$. Hence the raw stochastic fluctuation is invisible at the original scale, and a nondegenerate Gaussian limit is recovered only after centering and rescaling by $\sqrt{b/\eta}$. This is the standard stochastic-approximation functional CLT regime; the diffusion lives on the fluctuation scale, not in the raw iterate path.

5.4 The OU regime as the equilibrium specialization

Suppose θ^* is a stationary point: $h(\theta^*) = 0$, and $\theta_0 = \theta^*$ so that the ODE flow is trivial, $\bar{\theta}(t) \equiv \theta^*$. Then the drift coefficient in (26) is the constant matrix $H^* := \nabla h(\theta^*) = \nabla^2 L(\theta^*)$, and the diffusion coefficient is the constant matrix $C^*(\theta^*)$.

Assumption 5.9 (Nondegeneracy at θ^*). $H^* \succ 0$ and $G^*(\theta^*) \succ 0$.

Theorem 5.10 (OU fluctuation limit at a stationary point). *Under Assumption 5.9 and the conditions of Theorem 5.7 with $\theta_0 = \theta^*$, the fluctuation limit U of Theorem 5.7 solves the Ornstein–Uhlenbeck SDE*

$$dU_t = -H^* U_t dt + C^*(\theta^*) dW_s, \quad C^*(\theta^*) C^*(\theta^*)^\top = G^*(\theta^*). \quad (32)$$

Equivalently, on the original iterate scale, the centered iterate $\hat{\theta}^\eta(t) - \theta^$ admits the asymptotic expansion*

$$\hat{\theta}^\eta(t) - \theta^* = \sqrt{\frac{\eta}{b}} U_t + o_{\mathbb{P}}(\sqrt{\frac{\eta}{b}}).$$

Proof. Specialize (26) to $\bar{\theta}(\cdot) \equiv \theta^*$: the drift becomes $-H^* U_t$ and the diffusion becomes $C^*(\theta^*) dW_t$. The original-scale expansion is (27) with $\bar{\theta} \equiv \theta^*$. \square

Corollary 5.11 (Fluctuation-scale Lyapunov equation and discrete-scale benchmark). *Under Assumption 5.9, the OU process (32) is exponentially ergodic with stationary law $\mathcal{N}(0, \Sigma_U)$, where Σ_U is the unique symmetric positive definite solution of the fluctuation-scale Lyapunov equation*

$$H^* \Sigma_U + \Sigma_U (H^*)^\top = G^*(\theta^*). \quad (33)$$

On the original iterate scale, Proposition 5.13 provides a discrete Lyapunov covariance Σ_η^{lin} for the linearized recursion, which at leading order in η equals $(\eta/b)\Sigma_U$ and satisfies

$$H^* \Sigma_\eta^{\text{lin}} + \Sigma_\eta^{\text{lin}} (H^*)^\top = \frac{\eta}{b} G^*(\theta^*) + O(\eta) \cdot \Sigma_\eta^{\text{lin}}. \quad (34)$$

This is the linearized-recursion benchmark on the original iterate scale; we do not claim an invariant law for the nonlinear SGD iterates here. Because H^* is symmetric positive definite, cyclicity of trace gives the unconditional trace identity

$$2 \text{Tr}(\Sigma_U) = \text{Tr}((H^*)^{-1} G^*(\theta^*)). \quad (35)$$

Proof. Write $B := (G^*(\theta^*))^{1/2}$, so $BB^\top = G^*(\theta^*)$. Since $H^* \succ 0$, $-H^*$ is Hurwitz and the OU process is exponentially ergodic with stationary law $\mathcal{N}(0, \Sigma_U)$. Applying Itô's formula to $U_t U_t^\top$ and taking stationary expectations yields $-(H^* \Sigma_U + \Sigma_U H^{*\top}) + BB^\top = 0$, which is (33); the integral representation $\Sigma_U = \int_0^\infty e^{-H^* s} G^*(\theta^*) e^{-H^{*\top} s} ds$ converges and gives uniqueness (Lemma A.1). Equation (34) follows from Proposition 5.13 after dividing out leading powers of η (Remark 5.14). The trace identity follows by left-multiplying (33) by $(H^*)^{-1}$ and using $\text{Tr}(H^{-1} \Sigma H) = \text{Tr}(\Sigma)$. \square

Remark 5.12 (Likelihood specialization). When $\ell(\theta; z) = -\log p_\theta(z)$ and the model is correctly specified, $G^*(\theta^*) = F^*(\theta^*)$. The fluctuation-scale Lyapunov equation (33) then reads $H^* \Sigma_U + \Sigma_U H^{*\top} = F^*(\theta^*)$; the linearized discrete-recursion benchmark of Proposition 5.13 satisfies $\Sigma_\eta^{\text{lin}} = (\eta/b)\Sigma_U + o(\eta/b)$ at leading order in η (Corollary 5.11). Fisher geometry is therefore explicit both in the transient fluctuations and in the linearized stationary Lyapunov balance; we do not assert an invariant law for the nonlinear SGD iterates here.

5.5 Discrete-time stationary covariance: an exact bridge

The same G^* that governs the fluctuation-scale Lyapunov equation (33) also governs the exact linearized discrete-time stationary covariance. The continuous-time identity (34) is the small- η reduction of the discrete Lyapunov equation below.

Proposition 5.13 (Discrete-time linearized stationary covariance). *Consider the linearized discrete-time recursion around θ^* with constant stepsize η and batch size b :*

$$\Delta_{t+1} = (I - \eta H^*) \Delta_t + \eta \zeta_{t+1}, \quad \mathbb{E}[\zeta_{t+1} \zeta_{t+1}^\top \mid \mathcal{F}_t] = \frac{1}{b} G^*(\theta^*) + r_t, \quad (36)$$

where $\|r_t\|_{\text{op}} = o(b^{-1})$ as in (24). If $\rho(I - \eta H^*) < 1$ (equivalently, $\eta < 2/\lambda_{\max}(H^*)$), the linearized covariance recursion is stable and admits a unique stationary covariance $\Sigma_\eta := \lim_{t \rightarrow \infty} \text{Cov}(\Delta_t)$

satisfying the discrete Lyapunov equation

$$\Sigma_\eta = (I - \eta H^*) \Sigma_\eta (I - \eta H^*)^\top + \frac{\eta^2}{b} G^*(\theta^*), \quad (37)$$

up to the same local remainder terms already used in the fluctuation analysis.

Proof. From (36), $\text{Cov}(\Delta_{t+1}) = (I - \eta H^*) \text{Cov}(\Delta_t) (I - \eta H^*)^\top + \eta^2 \mathbb{E}[\zeta_{t+1} \zeta_{t+1}^\top | \mathcal{F}_t]$ using $\mathbb{E}[\zeta_{t+1} | \mathcal{F}_t] = 0$. Under $\rho(I - \eta H^*) < 1$, the map $\Sigma \mapsto (I - \eta H^*) \Sigma (I - \eta H^*)^\top + Q$ is a contraction on positive semidefinite matrices, so the covariance iteration converges to the unique fixed point (37). The spectral radius condition is equivalent to $0 < \eta < 2/\lambda_{\max}(H^*)$, since $H^* \succ 0$. The statement is about the second-moment recursion for the linearized iterates; geometric ergodicity of the nonlinear SGD iterates would require additional assumptions (drift + minorization) that we do not impose. \square

Remark 5.14 (Small-stepsize reduction and the continuous limit). Expanding (37), $H^* \Sigma_\eta + \Sigma_\eta H^{*\top} = (\eta/b)G^* + \eta H^* \Sigma_\eta H^{*\top}$. When $\eta \lambda_{\max}(H^*)$ is small, the $O(\eta)$ discretization correction is negligible, and the discrete equation reduces to the continuous-time, original-scale identity (34). The covariance identification $\mathbb{E}[\xi \xi^\top | \mathcal{F}] \approx b^{-1}G^*$ is logically prior to both: the discrete Lyapunov equation is its exact linearized consequence, and the continuous equation is the small- η reduction that matches the fluctuation-scale limit of Theorem 5.7 after multiplying back by η/b .

6 Convergence Rates in Fisher Geometry

This section establishes *matching* upper and lower bounds for SGD when the error is measured in a *frozen* Fisher metric at a local optimum θ^* . Once the mini-batch noise covariance is identified (Section 4), the remaining work is a localized stochastic-approximation argument in a fixed geometry, followed by an information-theoretic lower bound expressed in the same metric. *Convention.* All rates in this section are stated in the identified statistical risk $\mathbb{E}[\theta_T^\top F^* \theta_T]$ unless explicitly noted otherwise; any Euclidean norm that appears is immediately converted.

6.1 Local Fisher Geometry and a Frozen-Metric Regime

Work in a neighborhood of θ^* where the Fisher information varies slowly. For clean rate statements we freeze the metric

$$F^* := F(\theta^*), \quad \|v\|_{F^*}^2 := v^\top F^* v.$$

(Allowing a slowly varying metric $F(\theta)$ is standard via localization; the frozen-metric bounds below are the local core and are what we use later for oracle complexity.)

Lemma 6.1 (Sufficient condition for the frozen-metric regime). *Suppose $F(\theta)$ is Lipschitz on a neighborhood \mathcal{U} of θ^* : $\|F(\theta) - F(\theta^*)\|_{\text{op}} \leq L_F \|\theta - \theta^*\|_2$ for all $\theta \in \mathcal{U}$. If the SGD iterates*

satisfy $\|\theta_t - \theta^*\|_2 = o(1)$ almost surely, then for every $\epsilon > 0$ there exists t_0 such that for $t \geq t_0$, $(1 - \epsilon)F^* \preceq F(\theta_t) \preceq (1 + \epsilon)F^*$.

Let $h(\theta) := \nabla L(\theta)$ and decompose the mini-batch estimator as

$$g_t(\theta_t) = h(\theta_t) + \xi_t, \quad \mathbb{E}[\xi_t \mid \mathcal{F}_t] = 0,$$

where \mathcal{F}_t is the natural filtration. Under Fisher alignment (Section 4), the conditional covariance satisfies the local approximation

$$\mathbb{E}[\xi_t \xi_t^\top \mid \mathcal{F}_t] = \frac{1}{b} F^* + r_t, \quad \|r_t\|_{\text{op}} \leq \frac{c_r}{b} \rho_t, \quad (38)$$

with $\rho_t \rightarrow 0$ in the local regime.

Define the Fisher-strong-convexity constant at θ^* :

$$\mu_F := \lambda_{\min} \left(\frac{(F^*)^{1/2} H^* (F^*)^{-1/2} + (F^*)^{-1/2} H^* (F^*)^{1/2}}{2} \right), \quad H^* := \nabla^2 L(\theta^*). \quad (39)$$

Assumption 6.2 (Local coercivity in the frozen Fisher geometry). The constant μ_F defined in (39) is strictly positive. This is not automatic from $H^* \succ 0$ and $F^* \succ 0$ alone; it is an explicit compatibility condition between the loss curvature and noise geometry. It holds whenever H^* and F^* are jointly diagonalizable, and more generally whenever H^* and F^* are sufficiently aligned.

Define the effective dimension

$$d_{\text{eff}}(F^*) := \frac{\text{Tr}(F^*)}{\|F^*\|_{\text{op}}} = \frac{\text{Tr}(F^*)}{\lambda_{\max}(F^*)} \in (0, d]. \quad (40)$$

Remark 6.3 (Effective dimension as stable rank). The quantity $d_{\text{eff}}(F^*)$ is exactly the *stable rank* of F^* (Tropp, 2015): $d_{\text{eff}} \leq d$ always, with equality iff F^* is isotropic, and $d_{\text{eff}} \rightarrow 1$ when a single direction dominates. It replaces d in both the upper bound (Theorem 6.5) and the oracle complexity (Theorem 7.3), so that when Fisher information is concentrated ($d_{\text{eff}} \ll d$), the guarantees are correspondingly tighter than classical Euclidean bounds.

6.2 Upper Bound

Lemma 6.4 (One-step Fisher Lyapunov drift). Let $\Delta_t := \theta_t - \theta^*$ and $V_t := \|\Delta_t\|_{F^*}^2$. Assume: (i) L is locally M -smooth near θ^* ; (ii) $H^* \succ 0$; (iii) (38) holds. Then, as long as θ_t stays in the local neighborhood,

$$\mathbb{E}[V_{t+1} \mid \mathcal{F}_t] \leq \left(1 - 2\mu_F \eta_t + c_0 \eta_t^2\right) V_t + \eta_t^2 \frac{1}{b} \text{Tr}((F^*)^2) + \eta_t^2 \frac{c_1}{b} \text{Tr}(F^*) \rho_t, \quad (41)$$

where c_0, c_1 depend only on $(M, \|F^*\|_{\text{op}}, c_r)$.

Proof. From $\theta_{t+1} = \theta_t - \eta_t(h(\theta_t) + \xi_t)$, $\Delta_{t+1} = \Delta_t - \eta_t h(\theta_t) - \eta_t \xi_t$. Expanding $V_{t+1} = \Delta_{t+1}^\top F^* \Delta_{t+1}$ and taking conditional expectation (using $\mathbb{E}[\xi_t | \mathcal{F}_t] = 0$) yields

$$\mathbb{E}[V_{t+1} | \mathcal{F}_t] = V_t - 2\eta_t \Delta_t^\top F^* h(\theta_t) + \eta_t^2 h(\theta_t)^\top F^* h(\theta_t) + \eta_t^2 \text{Tr}(F^* \mathbb{E}[\xi_t \xi_t^\top | \mathcal{F}_t]).$$

Using $h(\theta^* + \Delta) = H^* \Delta + o(\|\Delta\|)$, we have $\Delta_t^\top F^* h(\theta_t) = \Delta_t^\top F^* H^* \Delta_t + o(V_t)$. Writing $x_t := (F^*)^{1/2} \Delta_t$ gives $\Delta_t^\top F^* H^* \Delta_t = x_t^\top \text{Sym}((F^*)^{1/2} H^* (F^*)^{-1/2}) x_t \geq \mu_F V_t$. Local M -smoothness implies $h(\theta_t)^\top F^* h(\theta_t) \leq c_0 V_t$. For the noise term, plug (38):

$$\text{Tr}(F^* \mathbb{E}[\xi_t \xi_t^\top | \mathcal{F}_t]) = \frac{1}{b} \text{Tr}((F^*)^2) + \text{Tr}(F^* r_t).$$

Finally $|\text{Tr}(F^* r_t)| \lesssim \text{Tr}(F^*) \|r_t\|_{\text{op}} \leq (c_1/b) \text{Tr}(F^*) \rho_t$, giving (41). \square

Theorem 6.5 (Upper bound in frozen Fisher geometry). *Assume Lemma 6.4. Take $\eta_t = \eta_0/t$ with $\eta_0 > 1/(2\mu_F)$, and assume $\sum_{t \geq 1} \eta_t^2 \rho_t < \infty$. Then for all $T \geq 2$,*

$$\mathbb{E}[\|\theta_T - \theta^*\|_{F^*}^2] \leq \frac{C_1}{b} \cdot \frac{\text{Tr}((F^*)^2)}{\mu_F} \cdot \frac{1}{T} + C_2 \cdot \frac{\|\theta_1 - \theta^*\|_{F^*}^2}{T^{2\mu_F \eta_0}} + \frac{C_3}{b} \cdot \frac{\text{Tr}(F^*)}{T}, \quad (42)$$

where C_1, C_2, C_3 depend only on $(\eta_0, \mu_F, c_0, c_1)$.

Moreover, using $\text{Tr}((F^*)^2) \leq \lambda_{\max}(F^*) \text{Tr}(F^*)$, we obtain

$$\begin{aligned} \mathbb{E}[\|\theta_T - \theta^*\|_{F^*}^2] &\leq \frac{\tilde{C}_1}{b} \cdot \frac{\lambda_{\max}(F^*) \text{Tr}(F^*)}{\mu_F} \cdot \frac{1}{T} + \tilde{C}_2 \cdot \frac{\|\theta_1 - \theta^*\|_{F^*}^2}{T^{2\mu_F \eta_0}} \\ &= \frac{\tilde{C}_1}{b} \cdot \frac{\lambda_{\max}(F^*)^2}{\mu_F} \cdot \frac{d_{\text{eff}}(F^*)}{T} + \tilde{C}_2 \cdot \frac{\|\theta_1 - \theta^*\|_{F^*}^2}{T^{2\mu_F \eta_0}}. \end{aligned} \quad (43)$$

Proof. Take total expectations in (41) to obtain $\mathbb{E}[V_{t+1}] \leq a_t \mathbb{E}[V_t] + u_t$ with $a_t := 1 - 2\mu_F \eta_t + c_0 \eta_t^2$ and $u_t := \eta_t^2 \frac{1}{b} \text{Tr}((F^*)^2) + \eta_t^2 \frac{c_1}{b} \text{Tr}(F^*) \rho_t$. Fix any $\epsilon \in (0, 2\mu_F)$. For $\eta_t = \eta_0/t$ and t large enough that $c_0 \eta_0^2/t \leq \epsilon \eta_0$, we have $a_t \leq 1 - (2\mu_F - \epsilon) \eta_0/t$; set $\alpha := (2\mu_F - \epsilon) \eta_0$, which satisfies $\alpha > 1$ whenever $\eta_0 > 1/(2\mu_F)$ and ϵ is chosen small enough. Define $A_{t,T} := \prod_{s=t}^{T-1} a_s$ (Lemma A.2). Unrolling gives $\mathbb{E}[V_T] \leq A_{1,T} V_1 + \sum_{t=1}^{T-1} A_{t+1,T} u_t$. With the consistent exponent α , the product bounds are $A_{1,T} \leq C T^{-\alpha}$ and $A_{t+1,T} \leq C (t/T)^\alpha$. Since $\alpha > 1$, the standard Robbins–Monro calculation gives $\sum_{t=1}^{T-1} A_{t+1,T} \eta_t^2 = O(1/T)$, yielding the leading $(\text{Tr}((F^*)^2)/b)(1/T)$ term. The remainder contribution is controlled because $\sum_t \eta_t^2 \rho_t < \infty$ and $A_{t+1,T} \leq 1$, adding $O((\text{Tr}(F^*)/b)(1/T))$. The transient term $A_{1,T} V_1 = O(T^{-\alpha})$ appears in the bound (42) with exponent $\alpha \leq 2\mu_F \eta_0$; sending $\epsilon \downarrow 0$ gives the exponent $2\mu_F \eta_0$ stated in (42) up to an arbitrarily small loss. The reduction to (43) follows from $\text{Tr}((F^*)^2) \leq \lambda_{\max}(F^*) \text{Tr}(F^*)$. \square

Remark 6.6 (Consistency with the OU viewpoint). The $1/(Tb)$ scaling in the frozen Fisher norm is consistent with the OU/Lyapunov stationary analysis: both predict the same leading-order

dependence on temperature $\tau = \eta/b$ and intrinsic curvature μ_F .

6.3 Lower Bound

We state the clean lower bound in the local parametric Fisher setting with i.i.d. observations. Extensions to adaptive oracles and general losses require additional machinery and are left as discussion (Remarks 6.11–6.12).

Assumption 6.7 (Local parametric regularity for van Trees). Let $\{P_\theta : \theta \in \Theta_{\text{loc}}\}$ be a parametric family on a neighborhood Θ_{loc} of θ^* with densities p_θ . Assume:

- (i) $\theta \mapsto p_\theta(z)$ is twice continuously differentiable for a.e. z ;
- (ii) the Fisher information $F(\theta) := \mathbb{E}_\theta[s_\theta s_\theta^\top]$ is continuous and positive definite on Θ_{loc} ;
- (iii) $\int \|s_\theta(z)\|^2 p_\theta(z) dz$ is uniformly bounded on Θ_{loc} ;
- (iv) there exists a smooth prior density π supported on Θ_{loc} with finite Fisher information $J_\pi := \int \|\nabla \log \pi(\theta)\|^2 \pi(\theta) d\theta < \infty$.

Proposition 6.8 (Local i.i.d. Fisher-case lower bound via van Trees). *Suppose Assumption 6.7 holds. Consider the local estimation model in which, for each $\theta \in \Theta_{\text{loc}}$, one observes N i.i.d. samples from P_θ and forms an estimator $\hat{\theta}_N$ (a measurable function of the samples). Then*

$$\inf_{\hat{\theta}_N} \sup_{\theta \in \Theta_{\text{loc}}} \mathbb{E}_\theta \left[\|\hat{\theta}_N - \theta\|_{F(\theta)}^2 \right] \geq \frac{c_{\text{loc}} d}{N}, \quad (44)$$

for a constant $c_{\text{loc}} > 0$ that depends on the local regularity of $F(\theta)$ on Θ_{loc} and on the prior regularity J_π from Assumption 6.7(iv). In particular, if each SGD iteration uses a fresh mini-batch of size b (so $N = Tb$ fresh-sample gradient calls), the Fisher-metric risk is bounded below by $c_{\text{loc}} d/(Tb)$ on the i.i.d. population oracle.

Proof. Standard van Trees argument (Gill and Levit, 1995). By Assumption 6.7(ii), the per-coordinate local Fisher scale $\bar{f} := \sup_{\theta \in \Theta_{\text{loc}}} \text{Tr} F(\theta)/d < \infty$ is N -independent. Fix a smooth prior π on Θ_{loc} with finite J_π (Assumption 6.7(iv)); the van Trees inequality for the Fisher-weighted Bayes risk gives $r_\pi(\hat{\theta}_N) \geq d/(N\bar{f} + J_\pi/d)$, and for $N \geq N_0 := J_\pi/(d\bar{f})$ the denominator is at most $2N\bar{f}$, yielding $r_\pi(\hat{\theta}_N) \geq c_{\text{loc}} d/N$ with $c_{\text{loc}} := 1/(2\bar{f}) > 0$ depending only on the local regularity of $F(\theta)$ on Θ_{loc} and independent of both N and d . Minimax risk dominates Bayes risk for any such prior, proving (44). \square

Remark 6.9 (Noise-covariance condition used in the upper bounds). The upper bounds of Theorem 6.5 and the oracle complexity of Theorem 7.3 use the conditional-covariance bound $\mathbb{E}[\xi_t \xi_t^\top | \mathcal{F}_t] \preceq b^{-1} F^*$, which is exactly the fresh-sampling specialization of Theorem 4.3 in the correctly specified likelihood case. No structure beyond this covariance identification is required.

Remark 6.10 (Rate matching, not geometry matching). Proposition 6.8 establishes a lower bound of rate order $\Omega(d/N)$ in the i.i.d. parametric Fisher setting. The quantities d_{eff} and κ_F appear only in the upper bound and oracle complexity (Theorems 6.5 and 7.3), not in the lower bound. Accordingly, we claim rate-order matching in the local Fisher case; we do *not* claim that the lower bound matches the geometry dependence of the upper bound.

Remark 6.11 (Adaptive-oracle and general-loss extensions). Two natural extensions of Proposition 6.8 are left to future work. (a) *Adaptive oracles*. A sequential oracle transcript $Y_t = \psi(\theta_t; Z_t)$ with a predictable per-step Fisher-information bound should yield (44) through a sequential van Trees argument, provided one establishes a uniform chain-rule bound on the joint transcript likelihood (requiring regularity conditions such as uniform local asymptotic equicontinuity that we do not develop here). (b) *General losses*. A local asymptotic normality (LAN) condition at θ^* with Godambe information $J_{\text{God}}(\theta^*) = H^{\star\top} G^{\star-1} H^*$ would produce a sandwich analogue of (44); see Le Cam (1986) and van der Vaart (1998).

Remark 6.12 (Legacy labels for cross-references). These labels are retained for backward compatibility; the i.i.d. Fisher lower bound is Proposition 6.8, and the general-loss extension is discussed in Remark 6.11.

Corollary 6.13 (Matching rate order in the local Fisher case). *Under Theorem 6.5 and the noise identification of Theorem 4.3 in the correctly specified likelihood setting,*

$$\mathbb{E}\left[\|\theta_T - \theta^*\|_{F^*}^2\right] = \Theta\left(\frac{1}{N}\right), \quad N = Tb,$$

at the level of rate order. Dependence on intrinsic geometry (d_{eff}, κ_F) appears only in the upper bound.

7 Oracle Complexity

This section records a standard high-probability conversion of the Fisher-geometry mean-square bounds of Section 6 into an oracle-complexity guarantee for ε -stationarity in the Fisher dual norm. The proof is a textbook descent-lemma plus martingale concentration argument (cf. Nesterov, 2004; Wainwright, 2019, Ch. 2); the novelty is not the complexity theorem itself but the fact that, once the mini-batch covariance is identified as $b^{-1}F^*$ (Theorem 4.3), the resulting constants read as intrinsic statistical quantities (κ_F, d_{eff}) rather than as Euclidean conditioning.

Throughout, we work locally near θ^* and freeze the metric $F^* := F(\theta^*) \succ 0$ (for general losses, replace F^* by $G^*(\theta^*)$; see Remark 7.5).

7.1 Stationarity in the Fisher dual norm

Definition 7.1 (ε -stationarity in Fisher dual norm). Let $F^\star \succ 0$. We say θ is ε -stationary (in the Fisher metric) if

$$\|\nabla L(\theta)\|_{(F^\star)^{-1}} := \sqrt{\nabla L(\theta)^\top (F^\star)^{-1} \nabla L(\theta)} \leq \varepsilon.$$

7.2 From Fisher distance to Fisher-dual stationarity

Lemma 7.2 (Distance-to-stationarity conversion). Assume L is M -smooth on a neighborhood \mathcal{U} of θ^\star and $F^\star \succ 0$. Then for all $\theta \in \mathcal{U}$,

$$\|\nabla L(\theta)\|_{(F^\star)^{-1}}^2 \leq \frac{M^2}{\lambda_{\min}(F^\star)^2} \|\theta - \theta^\star\|_{F^\star}^2. \quad (45)$$

Moreover, if $\theta \rightarrow \theta^\star$ and $\nabla L(\theta) = H^\star(\theta - \theta^\star) + o(\|\theta - \theta^\star\|)$, then locally

$$\|\nabla L(\theta)\|_{(F^\star)^{-1}}^2 \leq (1 + o(1)) \lambda_{\max}(F^{\star-1/2} H^\star F^{\star-1/2})^2 \|\theta - \theta^\star\|_{F^\star}^2. \quad (46)$$

Proof. By M -smoothness and $\nabla L(\theta^\star) = 0$, $\|\nabla L(\theta)\|_2 \leq M\|\theta - \theta^\star\|_2$. The dual-norm bound $\|v\|_{(F^\star)^{-1}}^2 \leq \lambda_{\min}(F^\star)^{-1} \|v\|_2^2$ converts Euclidean gradient norm to Fisher dual norm, and $\|\theta - \theta^\star\|_2^2 \leq \lambda_{\min}(F^\star)^{-1} \|\theta - \theta^\star\|_{F^\star}^2$ converts Fisher distance to Euclidean. Combining: $\|\nabla L\|_{(F^\star)^{-1}}^2 \leq \lambda_{\min}(F^\star)^{-1} M^2 \lambda_{\min}(F^\star)^{-1} \|\theta - \theta^\star\|_{F^\star}^2 = M^2 / \lambda_{\min}(F^\star)^2 \cdot \|\theta - \theta^\star\|_{F^\star}^2$. The local refinement follows by replacing M by $\|H^\star\|_{\text{op}}$ up to $1 + o(1)$ via the linearization. \square

7.3 High-probability oracle complexity

Theorem 7.3 (High-probability oracle complexity under the identified noise covariance). Assume the local regularity conditions of Section 3 hold on a neighborhood \mathcal{U} of θ^\star , and suppose that on \mathcal{U} the mini-batch noise is Fisher-aligned in the sense that, for some batch size $b \geq 1$,

$$\mathbb{E}[\xi_t | \mathcal{F}_t] = 0, \quad \mathbb{E}[\xi_t \xi_t^\top | \mathcal{F}_t] \preceq \frac{1}{b} F^\star. \quad (47)$$

Additionally, assume conditional sub-Gaussianity of the noise: for all $v \in \mathbb{R}^d$ with $\|v\| = 1$ and all $\lambda \in \mathbb{R}$, $\mathbb{E}[\exp(\lambda v^\top \xi_t) | \mathcal{F}_t] \leq \exp(\lambda^2 \|F^\star\|_{\text{op}} / (2b))$ a.s. (This is satisfied, for example, when per-sample gradients are almost surely bounded on \mathcal{U} .) Run SGD with constant batch size b and constant stepsize $\eta \leq 1/(4M)$:

$$\theta_{t+1} = \theta_t - \eta(\nabla L(\theta_t) + \xi_t).$$

Define the Fisher condition number and intrinsic dimension

$$\kappa_F := \frac{\lambda_{\max}(F^\star)}{\lambda_{\min}(F^\star)}, \quad d_{\text{eff}}(F^\star) := \frac{\text{Tr}(F^\star)}{\lambda_{\max}(F^\star)}.$$

Then there exists a universal constant $C > 0$ such that, for any $\delta \in (0, 1)$, with probability at least $1 - \delta$,

$$\min_{0 \leq t \leq T-1} \|\nabla L(\theta_t)\|_{(F^*)^{-1}}^2 \leq C \left(\frac{L(\theta_0) - L(\theta^*)}{\eta T \lambda_{\min}(F^*)} + \frac{\eta}{b} \kappa_F d_{\text{eff}}(F^*) \right) \log \frac{1}{\delta}. \quad (48)$$

In particular, balancing the two terms on the right-hand side over η yields

$$\min_{0 \leq t \leq T-1} \|\nabla L(\theta_t)\|_{(F^*)^{-1}}^2 \leq C' \sqrt{\frac{\kappa_F d_{\text{eff}}(F^*) (L(\theta_0) - L(\theta^*))}{N \lambda_{\min}(F^*)}} \log \frac{1}{\delta},$$

where $N = Tb$. Hence the squared Fisher-dual stationarity gap decays as $N^{-1/2}$, and to achieve $\min_{t < T} \|\nabla L(\theta_t)\|_{(F^*)^{-1}} \leq \varepsilon$ with probability at least $1 - \delta$ it suffices that

$$N = \Theta \left(\frac{\kappa_F d_{\text{eff}}(F^*) (L(\theta_0) - L(\theta^*))}{\lambda_{\min}(F^*) \varepsilon^4} \log^2 \frac{1}{\delta} \right). \quad (49)$$

The ε^{-4} rate is the standard nonconvex-SGD rate for squared-gradient stationarity at level ε^2 ; it is not the ε^{-2} rate of (strongly) convex stochastic optimization.

Proof. Step 1 (descent inequality, correct sign). By M -smoothness, $L(\theta_{t+1}) \leq L(\theta_t) + \langle \nabla L(\theta_t), \theta_{t+1} - \theta_t \rangle + \frac{M}{2} \|\theta_{t+1} - \theta_t\|^2$ with $\theta_{t+1} - \theta_t = -\eta(\nabla L(\theta_t) + \xi_t)$. Expanding $\|\nabla L(\theta_t) + \xi_t\|^2 = \|\nabla L(\theta_t)\|^2 + 2\langle \nabla L(\theta_t), \xi_t \rangle + \|\xi_t\|^2$,

$$L(\theta_{t+1}) \leq L(\theta_t) - \eta(1 - \frac{M\eta}{2}) \|\nabla L(\theta_t)\|^2 - \eta(1 - M\eta) \langle \nabla L(\theta_t), \xi_t \rangle + \frac{M\eta^2}{2} \|\xi_t\|^2.$$

Under $\eta \leq 1/(4M)$, $1 - M\eta/2 \geq 7/8$ and $1 - M\eta \geq 3/4$. Denote $\alpha := 1 - M\eta \in [3/4, 1)$.

Step 2 (define martingale). Let $\Delta M_{t+1} := -\eta\alpha \langle \nabla L(\theta_t), \xi_t \rangle$ and $M_T := \sum_{t=0}^{T-1} \Delta M_{t+1}$; since $\mathbb{E}[\xi_t | \mathcal{F}_t] = 0$, (M_t) is a martingale adapted to (\mathcal{F}_t) . Write $\Delta L := L(\theta_0) - L(\theta^*)$, $S_T := \sum_{t < T} \|\nabla L(\theta_t)\|^2$, and $Q_T := \sum_{t < T} \|\xi_t\|^2$. Summing the Step-1 inequality from $t = 0$ to $T - 1$,

$$\frac{7\eta}{8} S_T \leq \Delta L + M_T + \frac{M\eta^2}{2} Q_T. \quad (50)$$

Step 3 (Q_T tail via a Hanson–Wright-type bound). Under conditional sub-Gaussianity of ξ_t with variance proxy $\Sigma_t \preceq b^{-1}F^*$, the Hanson–Wright inequality for sub-Gaussian vectors (Vershynin, 2018, Thm. 6.2.1) gives, for an absolute constant c_0 , $\Pr(\|\xi_t\|^2 - \mathbb{E}[\|\xi_t\|^2 | \mathcal{F}_t] > s | \mathcal{F}_t) \leq 2 \exp(-c_0 \min\{s^2 b^2 / \|F^*\|_F^2, sb / \|F^*\|_{\text{op}}\})$; so $\|\xi_t\|^2 - \mathbb{E}[\|\xi_t\|^2 | \mathcal{F}_t]$ is conditionally sub-exponential with parameters $(\|F^*\|_F^2 / b^2, \|F^*\|_{\text{op}} / b)$. Applying Bernstein’s inequality (Wainwright, 2019, Ch. 2) over $t < T$ gives, with probability at least $1 - \delta/2$,

$$Q_T \leq \frac{T}{b} \text{Tr}(F^*) + c_1 \left(\frac{\|F^*\|_F}{b} \sqrt{T \log(2/\delta)} + \frac{\|F^*\|_{\text{op}}}{b} \log(2/\delta) \right). \quad (51)$$

Since $\|F^*\|_F^2 \leq d \|F^*\|_{\text{op}}^2$, the deviation term is $O(b^{-1} \sqrt{dT} \|F^*\|_{\text{op}} \sqrt{\log(1/\delta)})$, lower order than the

leading $(T/b)\text{Tr}(F^*)$ when $T \gtrsim d \log(1/\delta)$.

Step 4 (two-sided martingale concentration). The scalar $\langle \nabla L(\theta_t) / \|\nabla L(\theta_t)\|, \xi_t \rangle$ is conditionally sub-Gaussian with parameter at most $\|F^*\|_{\text{op}}/b$, so ΔM_{t+1} is conditionally sub-Gaussian with parameter $v_t^2 := \eta^2 \alpha^2 \|\nabla L(\theta_t)\|^2 \|F^*\|_{\text{op}}/b$. The standard two-sided Azuma–Hoeffding/Freedman-type bound for conditionally sub-Gaussian martingale sums (Wainwright, 2019, Thm. 2.19) gives, with probability at least $1 - \delta/2$,

$$|M_T| \leq \sqrt{2 \sum_{t < T} v_t^2 \log(4/\delta)} = \eta \alpha \sqrt{\frac{2\|F^*\|_{\text{op}}}{b} S_T \log(4/\delta)}. \quad (52)$$

Step 5 (combine). On the intersection of the events in (51)–(52) (probability $\geq 1 - \delta$ by union bound), substitute into (50) and use $|M_T|$ in place of M_T :

$$\begin{aligned} \frac{\eta}{8} S_T &\leq \Delta L + \eta \sqrt{\frac{2\|F^*\|_{\text{op}}}{b} S_T \log(4/\delta)} + \frac{M\eta^2 T}{2b} \text{Tr}(F^*) \\ &\quad + c_2 \frac{M\eta^2 \|F^*\|_{\text{op}}}{b} \left(\sqrt{T \log(2/\delta)} + \log(2/\delta) \right). \end{aligned} \quad (53)$$

The last term scales as $\eta^2 \sqrt{T}/b$ (up to log factors), strictly lower order than the leading variance term $\eta^2 T \text{Tr}(F^*)/b$ once $T \gtrsim \log(1/\delta)$, and is absorbed into the constant C below. Solving the resulting quadratic inequality in $\sqrt{S_T}$ for $S_T/T \geq \min_{t < T} \|\nabla L(\theta_t)\|^2$ yields

$$\min_{t < T} \|\nabla L(\theta_t)\|^2 \leq C \left(\frac{\Delta L}{\eta T} + \frac{\eta}{b} \text{Tr}(F^*) \right) \log(4/\delta),$$

for a constant C depending only on M , c_0 , and c_1 .

Step 6 (Fisher dual norm). Use $\|v\|_{(F^*)^{-1}}^2 \leq \lambda_{\min}(F^*)^{-1} \|v\|_2^2$ and $\text{Tr}(F^*)/\lambda_{\min}(F^*) = \kappa_F d_{\text{eff}}(F^*)$:

$$\min_{t < T} \|\nabla L(\theta_t)\|_{(F^*)^{-1}}^2 \leq C \left(\frac{\Delta L}{\eta T \lambda_{\min}(F^*)} + \frac{\eta}{b} \kappa_F d_{\text{eff}}(F^*) \right) \log \frac{1}{\delta},$$

establishing (48). For (49), balance the two terms by taking $\eta^* = \sqrt{\Delta L b / (T \lambda_{\min}(F^*) \kappa_F d_{\text{eff}})}$, which gives the balanced RHS $\sim \sqrt{\Delta L \kappa_F d_{\text{eff}} / (T b \lambda_{\min})} \log(1/\delta)$, i.e., the squared-norm gap decays as $N^{-1/2}$ in $N = Tb$. Requiring this squared gap to be at most ε^2 yields the ε^{-4} scaling of (49). \square

Remark 7.4 (Statistical vs. Euclidean conditioning). Classical oracle-complexity results use the Hessian condition number κ_H and ambient dimension d ; here they are replaced by the Fisher counterparts κ_F and d_{eff} . The substitution is not cosmetic: a problem may be Euclidean-stiff ($\kappa_H \gg 1$) yet statistically well-conditioned ($\kappa_F = O(1)$) when curvature and information share the same eigenstructure; conversely, isotropic curvature does not guarantee favorable statistical complexity.

Remark 7.5 (General losses / Godambe geometry). For general losses, replace F^* by $G^*(\theta^*)$

throughout and interpret the dual norm accordingly. The alignment condition (47) is then exactly the local conclusion of Theorem 4.3.

Remark 7.6 (Iteration vs. oracle complexity). Equation (49) counts *oracle calls* $N = Tb$. If reporting iteration complexity, keep b explicit and interpret $T = N/b$.

Remark 7.7 (Interpreting the complexity constants). The product $\kappa_F d_{\text{eff}}$ in (49) measures the total cost of resolving all statistically relevant directions at the hardest direction’s scale (see Remark 6.3 for the role of d_{eff} as the stable rank of F^*). Equation (49) links the sampling budget N to achievable stationarity through intrinsic problem geometry.

Corollary 7.8 (Batch-size scaling under a fixed sample budget). *Fix a total sampling budget N and run $T = N/b$ iterations of constant-stepsize SGD with batch size b . Balancing the bias term $\sim (L(\theta_0) - L^*) / (\eta T \lambda_{\min}(F^*))$ and the variance term $\sim \eta \kappa_F d_{\text{eff}} / b$ in (48) yields the balanced stepsize $\eta^* \propto \sqrt{b / (T \kappa_F d_{\text{eff}})}$. Feasibility. The balanced stepsize must respect the theorem’s own step-size cap $\eta \leq 1/(4M)$. Substituting $T = N/b$ gives $\eta^* = b \sqrt{\Delta L / (N \lambda_{\min}(F^*) \kappa_F d_{\text{eff}})}$, so the cap $\eta^* \leq 1/(4M)$ imposes the feasibility condition*

$$b \leq \sqrt{\frac{N \lambda_{\min}(F^*) \kappa_F d_{\text{eff}}}{16 M^2 \Delta L}}.$$

The batch-invariance conclusion below is a statement within this feasibility region (so b may grow like \sqrt{N} , not linearly in N), not at arbitrary b . Substituting $T = N/b$ and taking $\eta = \eta^*$ within the feasibility region, the resulting squared Fisher-dual stationarity gap satisfies

$$\min_{t < T} \|\nabla L(\theta_t)\|_{(F^*)^{-1}}^2 = \mathcal{O}\left(\sqrt{\frac{\kappa_F d_{\text{eff}}}{N}}\right),$$

so the norm gap decays as $N^{-1/4}$. Within the feasibility region the bound is independent of b at leading order, which suggests—under a fixed oracle budget—that small batches do not degrade the worst-case guarantee while gaining more frequent iterates; the identified geometry determines the constant but not the scaling in N .

8 Numerical Validation

The empirical program is organized in three layers, each answering a distinct question about the identified covariance and its downstream consequences:

- (i) **Direct identification (Experiment 1).** Does $\text{Cov}(g_B(\theta^*)) \approx b^{-1} G^*(\theta^*)$ hold in an actual mini-batching setup—including under model misspecification, where curvature and noise geometry diverge?

- (ii) **Fluctuation-scale geometric illustrations (Experiment 2).** What does the Lyapunov structure implied by the identified covariance *look* like in a low-dimensional setting where individual eigendirections can be visualized?
- (iii) **Raw-scale quantitative validations (Experiments 3–6).** Do the original-iterate-scale predictions—discrete Lyapunov plateau at constant step, $1/N$ rate under Robbins–Monro schedules, directional amplification, and the fluctuation-scale (η/b) -collapse (signature of Theorem 5.7)—hold quantitatively in direct SGD on higher-dimensional problems?

Layer (i) is the direct check of Theorem 4.3. Layer (ii) is interpretive: it visualizes the fluctuation-scale Lyapunov geometry on the normalized time-changed OU process of Theorem 5.7, and is *not* a direct Monte Carlo verification of raw SGD. Layer (iii) carries the main empirical weight: Experiments 3–6 are direct SGD recursions on the original iterate scale, and are the quantitative counterparts of the Lyapunov, rate, directional, and scaling-collapse predictions derived in Sections 5–7. Additional robustness diagnostics (approximate exchangeability) are deferred to Appendix B; reproducibility details (seeds, shared parameters) are in the code archive.

8.1 Claim 1: The Mini-Batch Covariance Is Identified by the Sampling Design

Before probing downstream consequences, we verify the covariance identification of Theorem 4.3 directly.

8.1.1 Experiment 1: Direct Covariance Identification (Probit DGP, Logistic Fit).

We generate $n = 50,000$ observations from a probit data-generating process and fit a logistic model, so that the optimization target is the KL projection β^* rather than the true β_0 . Under misspecification the score covariance and curvature no longer coincide: $J^* := \text{Var}(\nabla_{\beta}\ell(\beta; X, Y)|_{\beta^*}) \neq H^* := \nabla^2\mathbb{E}[-\ell(\beta; X, Y)]|_{\beta^*}$. The covariance-identification theorem nevertheless predicts $\text{Cov}(g_B(\beta^*)) \approx b^{-1}J^*$, where J^* plays the role of $G^*(\theta^*)$ in the general-loss notation. We estimate J^* from the full-sample scores and compare its diagonal entries to those of the empirical mini-batch covariance (batch size $b = 256$, 800 replicates). Figure 2 shows close agreement (relative Frobenius difference ≈ 0.05): the identification holds even under misspecification, and mini-batch fluctuations are governed by the score covariance rather than by curvature alone.

8.2 Claim 2: The Lyapunov Geometry Is Visible in Low Dimensions

Once the identification is empirically in hand (Experiment 1), it is useful to visualize what the Lyapunov structure *looks like* in a two-dimensional setting before moving to the $d = 10$ quantitative tests. In the fluctuation-scale OU surrogate of Theorem 5.7, the stationary covariance Σ_U solves $H^*\Sigma_U + \Sigma_U H^{*\top} = G^*$, and Experiment 2 illustrates three consequences that are each most naturally

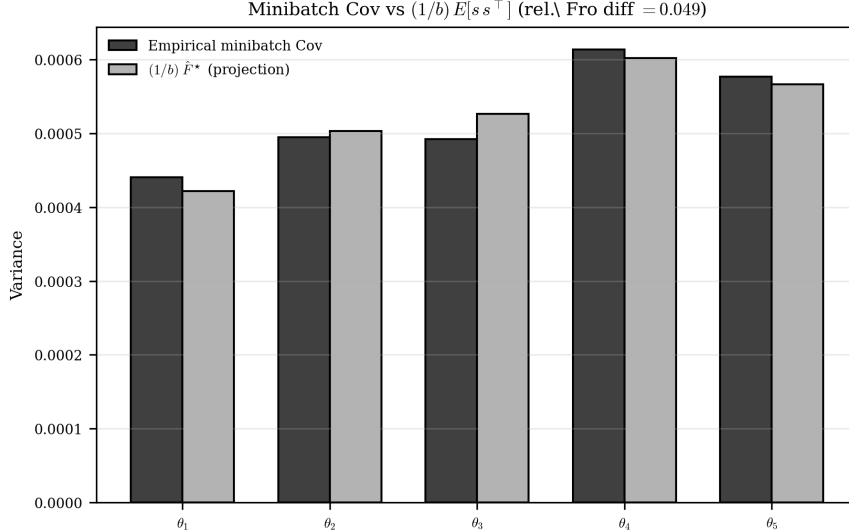


Figure 2: Experiment 1: direct covariance identification under misspecification (probit DGP, logistic fit). Diagonal entries of the empirical mini-batch covariance vs. $b^{-1}\hat{J}^*$ (projected score covariance at β^*); relative Frobenius difference ≈ 0.05 .

displayed in $d = 2$: the $1/b$ scaling of marginal variance, the redistribution of variance under curvature–noise misalignment, and the failure of trace-matched isotropic surrogates to reproduce directional structure. *These are interpretive illustrations, not direct quantitative validation of SGD*: the simulator integrates the time-changed OU process of (54) rather than running SGD iterates, and these subplots are included because a 2D visualization of the Lyapunov geometry aids intuition for the higher-dimensional quantitative tests that follow. The quantitative burden is carried by Experiments 3–6, which run direct SGD recursions.

8.2.1 Experiment 2: 2D Normalized OU Visualization of Lyapunov Structure.

For visualization we simulate a *pedagogical normalized OU process* chosen so that marginal variance scales as $1/b$ and is independent of η at leading order:

$$d\theta_t = -\eta H \theta_t dt + \sqrt{\frac{2\eta}{b}} F^{1/2} dW_t, \quad (54)$$

with $H = \text{diag}(1, 0.1)$ and varying noise shape F . This normalization is chosen for visualization only; it is *not* the literal fluctuation SDE of Theorem 5.7, which scales out the b -dependence into the $\sqrt{b/\eta}$ rescaled process U^η . At stationarity, the continuous-time Lyapunov equation for (54) reads $H\Sigma + \Sigma H = (2/b)F$, and the resulting marginal variances visualize the $1/b$ scaling, curvature–noise misalignment effects, and rotation diagnostics of the Lyapunov geometry in two dimensions.

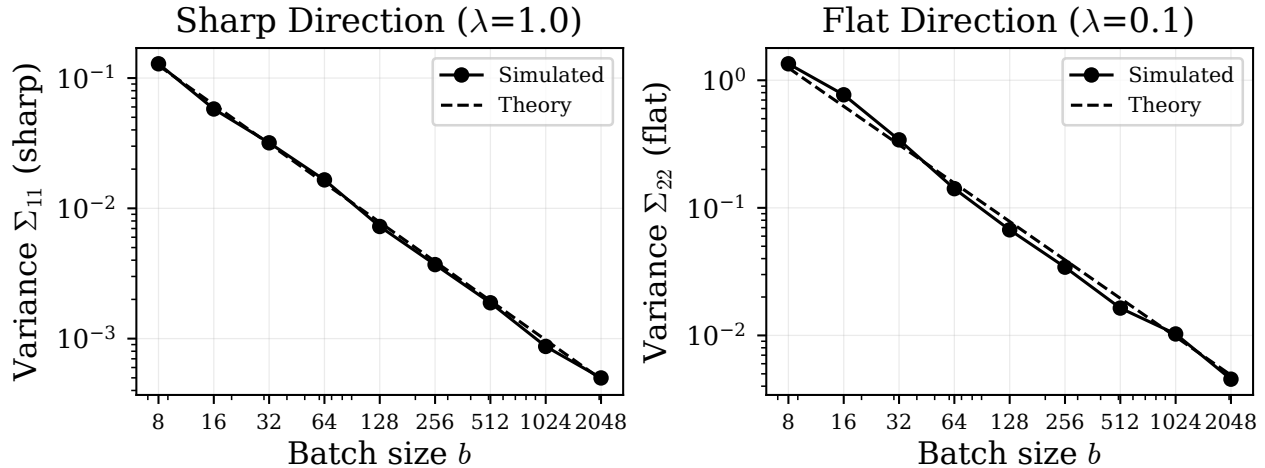


Figure 3: Experiment 2, 2D batch-size sweep: stationary variances vs. b (log scales); solid = simulation, dashed = fluctuation-scale Lyapunov prediction.

$$d = 2, H = \text{diag}(1, 0.1), F = I_2, 500 \text{ replicates, } 200\text{k steps.}$$

Batch-size sweep ($1/b$ scaling). With $F = I_2$ and a wide sweep of b , Figure 3 overlays simulated stationary variances with the fluctuation-scale Lyapunov prediction: clean $1/b$ scaling holds across the sweep, with the flat coordinate mixing more slowly (weaker curvature) but reaching the same equilibrium law.

Angle sweep (curvature–noise misalignment). Rotating an anisotropic noise matrix $F(\varphi) = R(\varphi)\text{diag}(1.5, 0.5)R(\varphi)^\top$ relative to the curvature basis, Figure 4 shows a predictable transfer of stationary variance across coordinates as φ varies: alignment governs which directions receive noise energy at equilibrium, even when the scalar temperature η/b is held fixed. The discrete Lyapunov benchmark tracks the simulation closely.

Rotation diagnostic (geometry vs. scalar temperature). We compare a geometric OU with rotating diffusion $F_\star(\varphi)$ against a trace-matched isotropic surrogate $\sigma^2 I$ with $\sigma^2 = \text{Tr}F_\star/d$. Figures 5–6 show that the geometric stationary covariance $\Sigma_F(\varphi)$ tilts with φ (nonzero cross-covariance, redistributed marginals), while the isotropic surrogate remains axis-aligned at all angles. This is the signature the trace-matched surrogate *cannot* reproduce, and is the low-dimensional preview of the directional amplification measured in $d = 10$ by Experiment 5.

8.3 Claim 3: The Lyapunov Plateau Holds Quantitatively in $d = 10$

The 2D experiments display the qualitative geometry; we now move to $d = 10$ for the first high-dimensional quantitative checkpoint. This is where the *quantitative* weight of the Lyapunov prediction is tested: Experiment 3 runs direct SGD on a $d = 10$ problem and asks whether the empirically

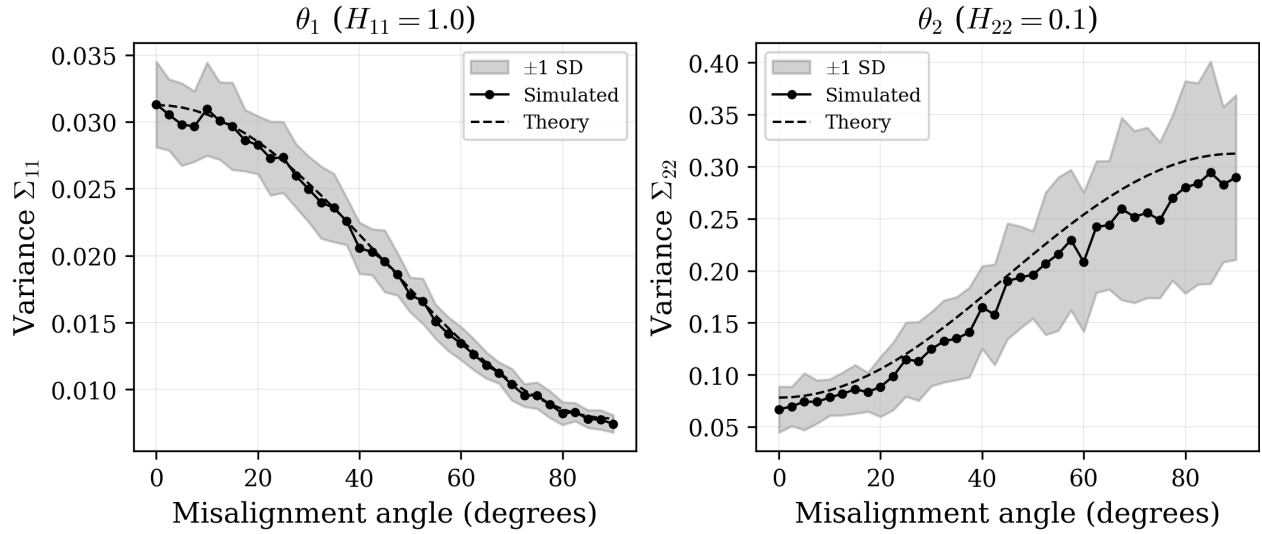


Figure 4: Experiment 2, 2D angle sweep: stationary variances vs. misalignment angle φ . Bands show replicate variability; dashed curves are the discrete Lyapunov prediction.

$d = 2$, $H = \text{diag}(1, 0.1)$, 500 replicates per angle.

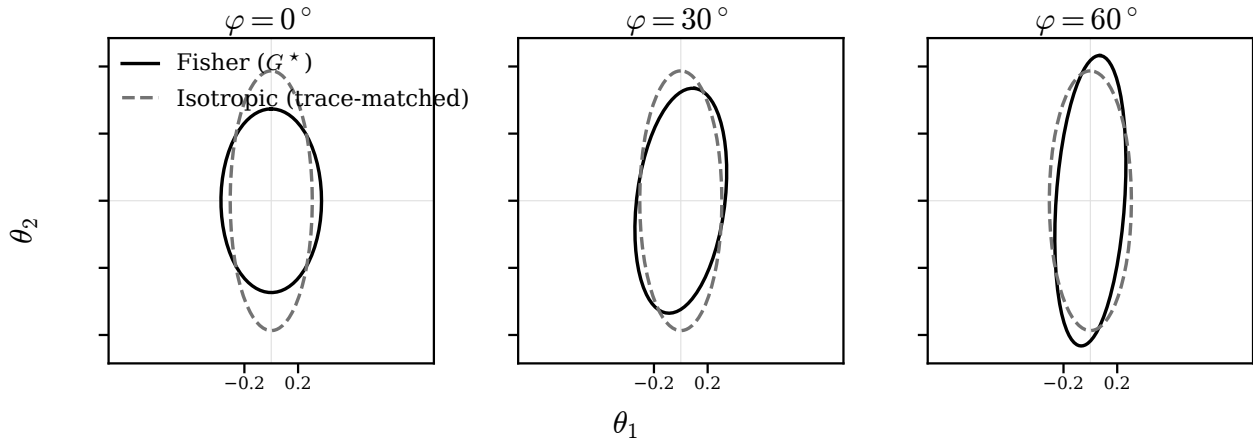


Figure 5: Experiment 2, 2D rotation diagnostic: stationary covariance ellipses at three rotation angles. The geometric equilibrium tilts with φ ; the isotropic trace-matched surrogate remains axis-aligned.

$d = 2$, $b = 64$; ellipses are 95% level sets of the Lyapunov solution.

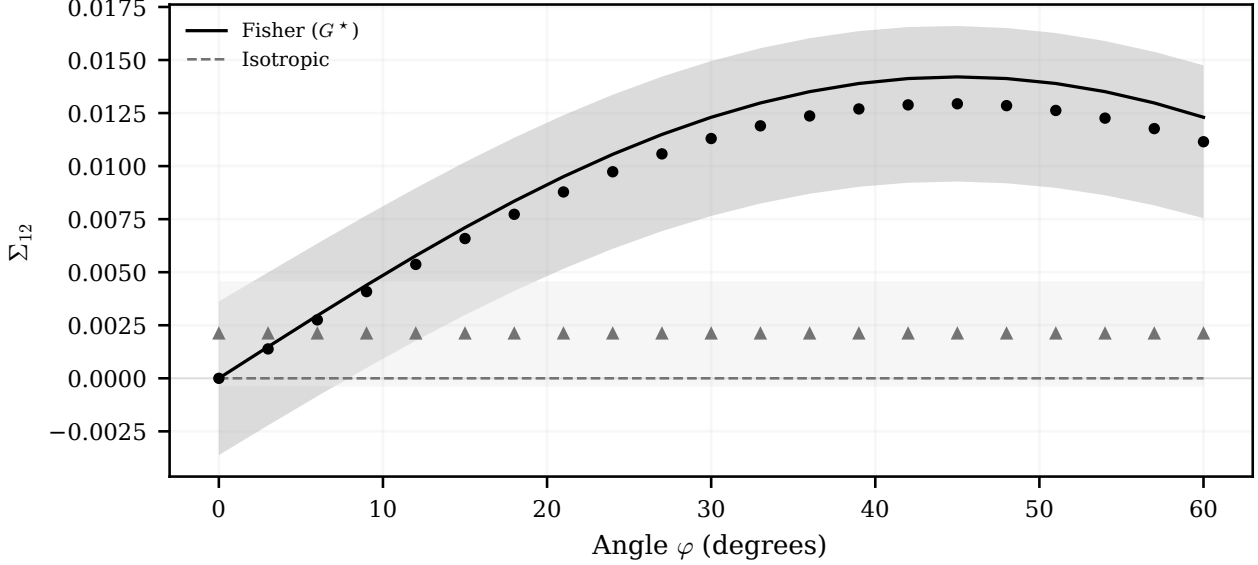


Figure 6: Experiment 2, 2D rotation diagnostic: cross-covariance Σ_{12} vs. rotation angle. Isotropic trace-matched noise fails to reproduce off-diagonal covariance; bands show ± 1 s.d. across seeds.

$d = 2$, 6 seeds, $T = 2,500$, burn-in = 800.

observed steady-state Fisher risk matches the level predicted by combining the identified covariance G^* with the discrete Lyapunov equation (Proposition 5.13). If the identification from Theorem 4.3 is quantitatively correct, both the anisotropic and isotropic empirical risks should converge to the Lyapunov-predicted plateau $\text{Tr}(F^*\Sigma_\eta^{\text{lin}})$ as T grows, with convergence ratios $\widehat{R}_T/R_\infty \rightarrow 1$.

8.3.1 Experiment 3: OU/Lyapunov Plateau in $d = 10$ (Anisotropic vs. Isotropic).

The curvature is $H = \text{diag}(\lambda_1, \dots, \lambda_{10})$ with eigenvalues log-spaced between 1 and 100, and we set $F^* = H^*$ throughout the synthetic $d = 10$ benchmark (the quadratic-Gaussian surrogate in which curvature and Fisher information coincide, so the Fisher-metric risk $\mathbb{E}[\|\theta_T\|_{F^*}^2]$ directly measures Hessian-weighted error). The noise shape G^* is a random SPD matrix with eigenvalues in $[0.5, 5]$, and we compare an isotropic control $G_{\text{iso}} = \sigma^2 I$ with $\sigma^2 = \text{Tr}(G^*)/d$ (trace-matched). Under constant step size $\eta = 0.5/\lambda_{\max}(H)$ and batch size $b = 64$, we run $R = 2,000$ replicates and record the Fisher-metric risk $\mathbb{E}[\|\theta_T\|_{F^*}^2]$ over increasing horizons $T \in \{300, 800, 2000, 5000, 10000\}$.

Table 3 confirms the Lyapunov prediction: both the anisotropic and isotropic empirical risks converge to the predicted stationary level as T grows, with convergence ratios \widehat{R}_T/R_∞ within 1% of unity across all horizons. The two plateaux nearly coincide because trace-matching is exact in this diagonal- H setting; the distinction between anisotropic and isotropic geometry is therefore invisible at the level of scalar risk, and only emerges in higher-order structure (Experiment 5).

T	Empirical Risk \widehat{R}_T		Lyapunov R_∞		\widehat{R}_T/R_∞	
	Aniso	Iso	Aniso	Iso	Aniso	Iso
300	8.55×10^{-4}	8.60×10^{-4}	8.63×10^{-4}	8.58×10^{-4}	0.991	1.002
800	8.64×10^{-4}	8.49×10^{-4}			1.002	0.990
2000	8.58×10^{-4}	8.50×10^{-4}			0.995	0.992
5000	8.72×10^{-4}	8.58×10^{-4}			1.010	1.001
10000	8.63×10^{-4}	8.47×10^{-4}			1.000	0.987

Table 3: Experiment 3 (OU/Lyapunov plateau, $d = 10$): empirical Fisher-metric risk vs. discrete Lyapunov prediction $R_\infty = \text{Tr}(F^* \Sigma_\eta^{\text{lin}})$. Convergence ratios $\widehat{R}_T/R_\infty \rightarrow 1$ confirm quantitative accuracy.

$d = 10$, $H = \text{diag}(1, \dots, 100)$, random G^* with eigenvalues in $[0.5, 5]$, $\eta = 0.5/\lambda_{\max}$, $b = 64$, $R = 2,000$ replicates.

8.4 Claim 4: Decaying Step Sizes Recover a $1/N$ Rate with a Geometry-Determined Constant

Under a Robbins–Monro step-size schedule the Fisher-metric risk decays as C/N where $N = Tb$ is the total oracle budget and the constant C is determined by the intrinsic geometry (G^*, H^*, F^*) . Specifically, the SA central-limit theorem gives an asymptotic covariance V satisfying $(\eta_0 H^* - \frac{1}{2}I)V + V(\eta_0 H^* - \frac{1}{2}I) = \frac{\eta_0^2}{b} G^*$, and $N \cdot \text{Risk} \rightarrow b \text{Tr}(F^* V)$. This is consistent with the upper bound (Theorem 6.5) in rate order and with the i.i.d. parametric Fisher lower-bound benchmark (Proposition 6.8).

8.4.1 Experiment 4: $1/N$ Rate and Fisher Constant (Decaying Step Size).

We switch to a decaying step size $\eta_t = \eta_0/(t+t_0)$ with $\eta_0 = 1.2$, $t_0 = 50$, and the same (H, G^*, G_{iso}) from Experiment 3, with oracle budget $N = Tb$ and $b = 64$. Figure 7 (left) plots the Fisher-metric risk on log–log axes: both anisotropic and isotropic risks decay as $1/N$ (fitted slopes ≈ -0.98), consistent with Theorem 6.5 in rate order. The right panel shows the scaled risk $N \cdot \widehat{\text{Risk}}$, which stabilizes near ≈ 14.2 (anisotropic) and ≈ 14.0 (isotropic)—both close to the SA–CLT prediction $b \text{Tr}(F^* V)$ where V solves the Lyapunov equation above.

Interpretation: two related-but-distinct constants. The constant-step Lyapunov quantity $\text{Tr}(G^* H^{*-1})$ (inset, ≈ 5.41) and the decaying-step asymptotic constant $b \text{Tr}(F^* V)$ (plateau, ≈ 14.0 – 14.2) are related but not identical: the former is the stationary $\text{Tr}(F^* \Sigma_\eta^{\text{lin}})$ of the constant-step discrete Lyapunov recursion at leading order in η , while the latter is the $N \rightarrow \infty$ asymptotic constant of the scaled risk under a Robbins–Monro schedule, which solves a *different* Lyapunov equation shifted by $-\frac{1}{2}I$. The shift reflects the variance deflation introduced by the decaying schedule. Both constants are determined by the identified geometry (G^*, H^*, F^*) , but their numerical values differ, and the ratio between them depends on the schedule (here $\eta_0 = 1.2$, $t_0 = 50$). The empirical scaled risk $N \cdot \widehat{\text{Risk}}$ lies above the i.i.d. parametric Fisher lower-bound benchmark of Proposition 6.8, consistent

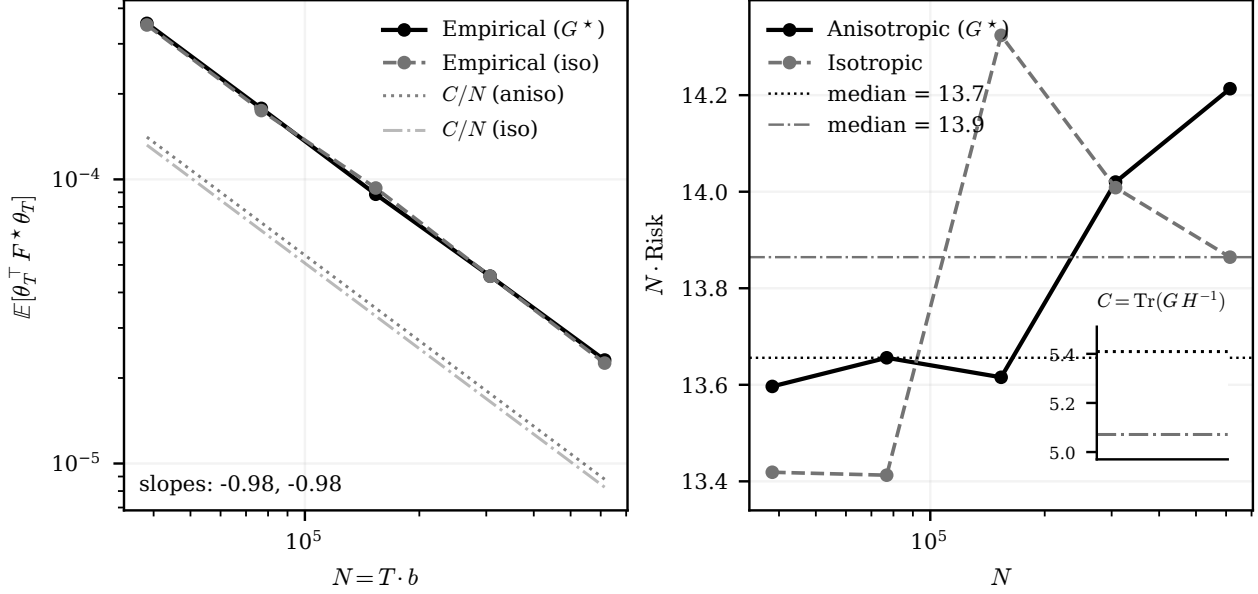


Figure 7: Experiment 4 (decaying step size, $d = 10$). **Left:** Fisher-metric risk vs. N (log-log); slopes ≈ -1 . **Right:** Scaled risk $N \cdot \text{Risk}$ stabilizes; inset shows $C = \text{Tr}(G^*H^{-1})$.

$$\eta_t = 1.2/(t + 50), b = 64, 800 \text{ replicates.}$$

with rate-order matching; we do not claim a specific value for the theorem constant.

8.5 Claim 5: Directional Amplification Discriminates Geometry from Scalar Temperature

Experiments 3 and 4 compared anisotropic and isotropic noise at the level of trace-scale summaries, where trace-matching makes the two surrogates nearly indistinguishable. This is precisely where scalar-temperature reasoning fails. In the synthetic benchmark $F^* = H^*$, so the plotted Fisher-metric risk is $\text{Tr}(F^*\Sigma) = \text{Tr}(H^*\Sigma)$. Multiplying the fluctuation-scale Lyapunov equation $H^*\Sigma_U + \Sigma_U H^{*\top} = G^*$ on the left by the identity and taking traces gives $2 \text{Tr}(H^*\Sigma_U) = \text{Tr}(G^*)$, which depends on G^* only through its trace; a trace-matched isotropic surrogate (G_{iso} with $\text{Tr}G_{\text{iso}} = \text{Tr}G^*$) therefore reproduces the scalar Fisher-risk summary by construction, even though its *directional* distribution of residual risk is entirely different. The discriminating signature is *directional*: anisotropic noise concentrates stationary risk along the top eigendirections of G^* , while the isotropic surrogate spreads residual error uniformly. Experiment 5 measures this direction-by-direction.

8.5.1 Experiment 5: Directional Variance Amplification.

For $k = 1, 2, 3$ we project θ_T onto the top eigenvectors v_k of G^* and compute the directional second moment $\mathbb{E}[\langle v_k, \theta_T \rangle^2]$ under the same decaying-step setup as Experiment 4. Figure 8 (left) shows

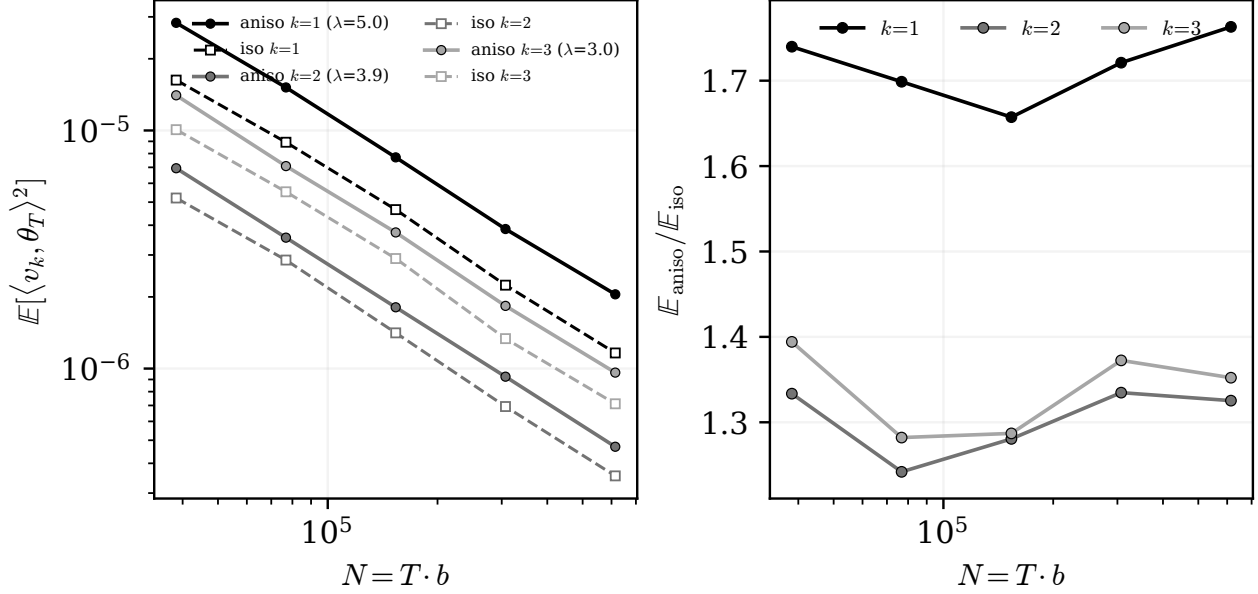


Figure 8: Experiment 5 (directional variance amplification, $d = 10$). **Left:** Directional second moments along top eigenvectors of G^* . **Right:** Ratio of anisotropic to isotropic directional variances; ratios > 1 mirror the eigenvalue ordering of G^* . Trace-matched isotropic noise preserves $\text{Tr}(G^*)$ but spreads residual risk uniformly; the identified anisotropic noise concentrates it along the top noise eigendirections.

Same setup as Experiment 4; top $k = 1, 2, 3$ eigenvectors of G^* .

that both models decay as $1/N$, but the anisotropic curve is systematically above the isotropic one along the top eigendirections. The right panel plots the ratio $\mathbb{E}_{\text{aniso}}/\mathbb{E}_{\text{iso}}$: at the largest budget the empirical ratios are $(1.76, 1.33, 1.35)$ for $k = 1, 2, 3$, close to the linearized Lyapunov prediction $(1.77, 1.40, 1.33)$ obtained from $H^*\Sigma_U + \Sigma_U H^{*\top} = G^*$. The ratios are strictly greater than one in every direction and largest along the top eigenvector of G^* . Trace-matched isotropic noise matches the scalar-risk summaries of Experiments 3–4 but cannot reproduce this direction-by-direction risk allocation; the identified geometry determines which parameter directions carry the most residual risk.

8.6 Claim 6: Fluctuation-Scale (η/b) -Collapse on the Raw Iterate Path

Theorem 5.7 and Corollary 5.11 predict that, in the small-stepsize local regime, $\mathbb{E}[\|\theta_T - \theta^*\|_{F^*}^2] = (\eta/b) \text{Tr}(F^*\Sigma_U) + o(\eta/b)$ with Σ_U solving $H^*\Sigma_U + \Sigma_U H^{*\top} = G^*(\theta^*)$. Equivalently, the scaled Fisher risk $(b/\eta) \widehat{\text{Risk}}$ should collapse to a single η, b -free curve at leading order. This is the direct empirical signature of the fluctuation FCLT (Theorem 5.7) on the original iterate scale.

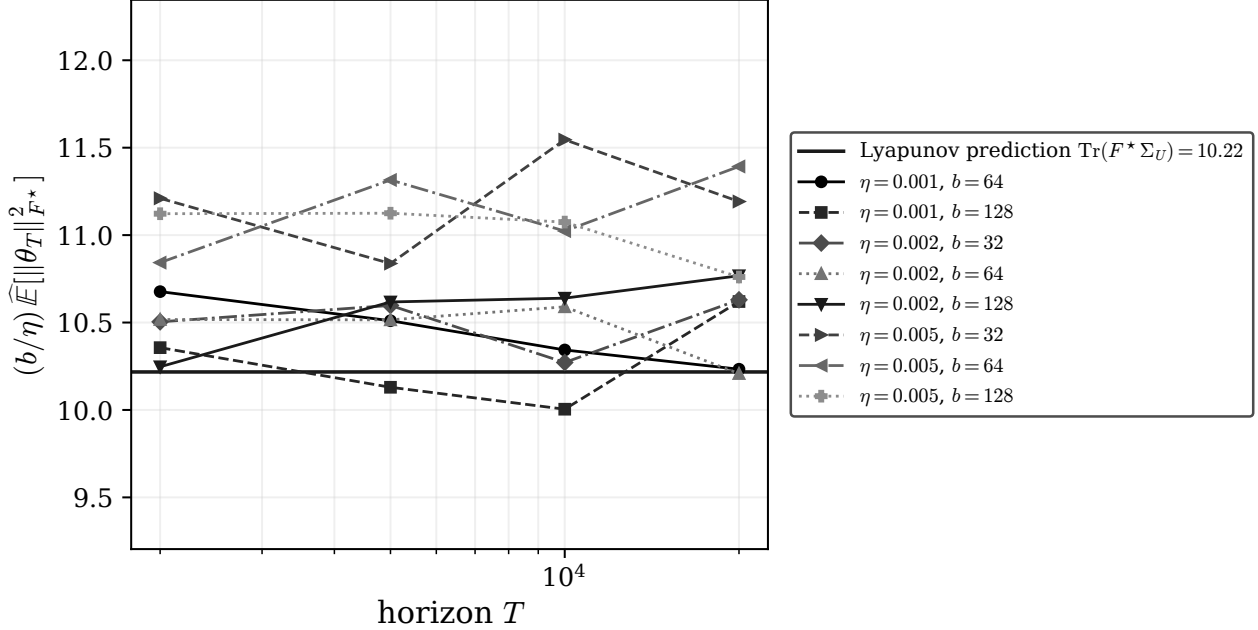


Figure 9: Experiment 6 (fluctuation-scale collapse diagnostic; Theorem 5.7): scaled Fisher risk $(b/\eta) \widehat{\mathbb{E}}[\|\theta_T\|_{F^*}^2]$ stabilizes at the fluctuation-scale Lyapunov prediction $\text{Tr}(F^*\Sigma_U)$ (black line) across eight (η, b) configurations.

$d = 10$, direct SGD, $R = 600$ replicates per cell; $\eta \in \{0.001, 0.002, 0.005\}$, $b \in \{32, 64, 128\}$.

8.6.1 Experiment 6: Raw-Scale Collapse Diagnostic.

We sweep eight (η, b) configurations with $\eta \in \{0.001, 0.002, 0.005\}$, $b \in \{32, 64, 128\}$ (so $\eta\lambda_{\max}(H^*) \in \{0.1, 0.2, 0.5\}$; $\eta/b \in [8 \times 10^{-6}, 1.6 \times 10^{-4}]$), and run direct SGD on the same (H, F^*, G^*) as Experiments 3–4 for $T \in \{2000, 5000, 10000, 20000\}$ with $R = 600$ replicates per cell. Figure 9 plots $(b/\eta) \widehat{\mathbb{E}}[\|\theta_T\|_{F^*}^2]$ against T for each configuration. All curves collapse onto a common plateau near $\text{Tr}(F^*\Sigma_U) \approx 10.22$ (black reference line), the fluctuation-scale Lyapunov prediction. The collapse across two orders of magnitude in η/b is a direct verification of the (η/b) -scaling law on the raw iterate scale, independently of any continuous-time normalization convention.

Additional robustness experiments under approximate exchangeability are reported in Appendix B.

9 Discussion

9.1 Summary of Contributions

The paper’s central contribution is operational: we identify the mini-batch gradient covariance from the sampling design itself as $b^{-1}G^*(\theta)$, converting the diffusion analysis of constant-step SGD

from a modeling exercise into a statement about the replication budget. In likelihood models the identified matrix reduces to projected Fisher information; in general losses it pairs with H^* through the classical sandwich/Godambe geometry of M-estimation. At fixed batch size, the raw iterate path has a deterministic fluid limit (the gradient-flow ODE); the $\sqrt{b/\eta}$ -scaled fluctuations converge to a linear diffusion with coefficient G^* ; near a nondegenerate optimum this is Ornstein–Uhlenbeck, and the corresponding Lyapunov covariance scaled by η/b matches the stationary covariance of the linearized discrete recursion at leading order. In the local Fisher case, an upper bound of order $1/N$ is rate-order matched by an i.i.d. van Trees lower bound, with the intrinsic dimension d_{eff} and statistical condition number κ_F appearing in the upper bound only.

9.2 Operational Implications for Sampling-Budget Design

The effective temperature $\tau = \eta/b$ is the single scalar that converts replication effort into diffusion amplitude, and the identification shows it does so in a *directional* way fixed by G^* rather than uniformly. For an OR practitioner, three consequences follow at the sampling-budget level. First, at a fixed oracle budget $N = Tb$, the batch size b trades iterate count against per-step noise scale: increasing b cools the error floor predicted by the linearized discrete Lyapunov benchmark (Proposition 5.13) in magnitude, but leaves the noise ellipsoid’s *shape* unchanged. Second, classical OR variance-reduction interventions (common variates, control variates, stratification) should be evaluated by their Loewner effect on G^* , and thus by the induced reduction in $\text{Tr}(Q\Sigma)$ for the operational metric Q , rather than by scalar component-variance alone—this is the natural bridge from classical variance-reduction practice to mini-batch SGD. Third, the directional amplification in Experiment 5 identifies exactly which parameter components absorb residual risk, and thus where additional sampling effort has the largest marginal return.

Remark 9.1 (Variance reduction as Fisher-metric risk reduction). A VR technique that reduces G^* to $\tilde{G} \preceq G^*$ in the Loewner order yields $\tilde{\Sigma}_\infty \preceq \Sigma_\infty$ via the Lyapunov balance, and hence lower Fisher-metric risk.

Plain SGD does not precondition the drift; natural-gradient methods do so by explicitly reweighting ∇L . We do not claim plain SGD is “natural-gradient-like” in the drift sense; rather, its linearized local equilibrium benchmark (Proposition 5.13) reflects the noise covariance G^* through the Lyapunov balance. The identification also suggests adaptive batching—increasing b (cooling) when marginal noise reduction is valuable, decreasing it when exploration matters.

9.3 Practical Notes and Extensions

The preceding theory identifies a small set of geometric primitives— H^* , G^* (or F^*), and $\tau = \eta/b$ —that govern both transient rates and stationary risk.

Our analysis freezes $F(\theta)$ locally at F^* . Validity can be assessed by monitoring $\delta_F(t) :=$

$\|F(\theta_t) - F^*\|_{\text{op}}/\|F^*\|_{\text{op}}$; in our experiments the Lyapunov predictions remain accurate from random starts, indicating early entry into the basin of Fisher geometry.

9.4 Estimating G^* in Practice

Where G^* is not analytically available, the empirical covariance of per-sample gradients $\hat{G}(\theta_t) = \frac{1}{m-1} \sum_i (\psi_i - \bar{\psi})(\psi_i - \bar{\psi})^\top$ is the natural plug-in and converges at the standard $O(1/\sqrt{m})$ rate in operator norm; for large d , a diagonal or rank- k streaming approximation suffices for the quantities (d_{eff} , dominant eigendirections, scale anisotropy) that enter the bounds. Given \hat{G} , one can diagnose whether isotropic temperature-matching is likely to fail (by checking whether \hat{G} is far from a scalar multiple of I) and compare candidate batch sizes through the predicted stationary covariance Σ_η of Proposition 5.13. A natural design heuristic (not proved here) is to regulate $\tau_t \propto 1/\lambda_{\max}(H(\theta_t))$ to avoid over-heating in stiff directions; when $d_{\text{eff}} \ll d$, the linearized local equilibrium of Proposition 5.13 concentrates on the identifiable subspace captured by Π_θ , which is where the identified geometry is nondegenerate.

9.5 Limitations and Future Work

Our sharpest statements use local linearization near a nondegenerate critical point; extending to nonconvex regimes requires controlling state-dependent curvature and relating intrinsic geometry to metastability. When $d \gg n$, the identified covariance may be low-rank, and a satisfactory theory should work on identifiable manifolds with appropriate pseudoinverses. Finally, preconditioners (Gauss–Newton, KFAC) reshape both drift and noise geometry; a joint control theory co-designing contraction and diffusion—potentially under communication constraints—would connect information geometry to OR-style variance allocation at scale.

The empirical design intentionally progresses from interpretable geometric diagnostics (direct covariance identification, 2D Lyapunov visualization) to quantitative raw-scale validation under direct SGD recursions in $d = 10$, culminating in the fluctuation-scale (η/b) -collapse (Experiment 6; signature of Theorem 5.7) on the original iterate path.

Code availability. All experiments in Section 8 and Appendix B are reproducible from the accompanying code archive (`Python_Codes/`), with master script `run_all.py`, explicit random seeds, and wall-clock under 5 minutes on a single CPU.

A Technical Lemmas

This appendix collects the auxiliary lemmas invoked by the main-text proofs. The finite-population covariance identity (Lemma 4.1) and score identities (Lemma 3.2) are stated and proved in the main

text; we only restate here the auxiliary results (Lyapunov representation, Robbins–Monro product bound) that are invoked in later proofs but are not part of the main-text spine.

A.1 Lyapunov equation solution

Lemma A.1 (Lyapunov equation solution). *Let $A \in \mathbb{R}^{d \times d}$ with all eigenvalues having strictly positive real part. Let $Q \succeq 0$. Then the continuous Lyapunov equation $A\Sigma + \Sigma A^\top = Q$ has the unique solution*

$$\Sigma = \int_0^\infty e^{-As} Q e^{-A^\top s} ds.$$

Proof. Convergence: Since all eigenvalues of A have positive real part, $\|e^{-As}\| \leq C e^{-\lambda s}$ for some $C, \lambda > 0$, ensuring convergence.

Verification: $A\Sigma + \Sigma A^\top = \int_0^\infty \frac{d}{ds} (-e^{-As} Q e^{-A^\top s}) ds = [-e^{-As} Q e^{-A^\top s}]_0^\infty = Q$.

Uniqueness: If Σ_1, Σ_2 both solve the equation, then $\Delta := \Sigma_1 - \Sigma_2$ satisfies $A\Delta + \Delta A^\top = 0$, whose only solution is $\Delta = 0$ when A has eigenvalues with positive real part. \square

A.2 Product bound for Robbins–Monro weights

Lemma A.2 (Product bound for Robbins–Monro weights). *Let $a > 1$ and $c_0 > 0$. Define*

$$\alpha_k := 1 - \frac{a}{k} + \frac{c_0}{k^2}, \quad \Pi_{s,T} := \prod_{k=s}^{T-1} \alpha_k.$$

Then for all T sufficiently large:

(i) $\Pi_{1,T} \leq CT^{-a}$ for a constant $C = C(a, c_0)$.

(ii) $\Pi_{t+1,T} \leq C(t/T)^a$ for $1 \leq t < T$.

Proof. Taking logarithms: $\log \alpha_k = \log(1 - a/k + c_0/k^2) = -a/k + O(1/k^2)$ for large k . Thus $\log \Pi_{s,T} = -a \sum_{k=s}^{T-1} k^{-1} + O(1) = -a(\log T - \log s) + O(1)$. Exponentiating: $\Pi_{s,T} = O((s/T)^a)$. For $s = 1$: $\Pi_{1,T} = O(T^{-a})$. For $s = t + 1$: $\Pi_{t+1,T} = O((t/T)^a)$. \square

B Robustness: A Stylized Variance-Inflation Perturbation

The following experiment probes one stylized perturbation of the fresh-sampling assumption of Theorem 4.3: a scalar variance-inflation factor $(1 + \varepsilon)$ on the mini-batch covariance, modeling mild departures from ideal exchangeability (weak dependence, partial sample reuse). This is a specific perturbation diagnostic, not a general robustness theorem. A direct check of the identification itself under model misspecification is in Experiment 1 of Section 8.1.1.

To model mild departures from ideal exchangeability (e.g., weak dependence, contamination, or partial reuse of samples), we inflate the intrinsic covariance by a factor $(1 + \varepsilon)$ in the linearized

surrogate: $\text{Cov}(\xi_t) = (1/b)(1 + \varepsilon) G^*(\theta^*)$, $\varepsilon \in [0, 1]$. This captures “extra correlation” as increased effective diffusion amplitude. Linearity of the Lyapunov operator then implies $\Sigma(\varepsilon) = (1 + \varepsilon)\Sigma(0)$, so every stationary marginal variance inflates linearly in ε . Figure 10 confirms this prediction: the entire stationary covariance scales as though the system had a higher effective temperature $\tau_{\text{eff}} = (1 + \varepsilon)\eta/b$. To first order, small exchangeability violations act like “heating” the Fisher–Lyapunov equilibrium.

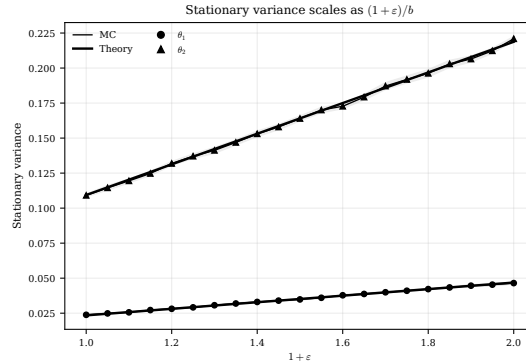


Figure 10: Experiment B: approximate exchangeability. Stationary variances vs. ε (simulation bands vs. linear Lyapunov prediction).

References

- Alekh Agarwal, Peter L. Bartlett, Pradeep Ravikumar, and Martin J. Wainwright. Information-theoretic lower bounds on the oracle complexity of stochastic convex optimization. *IEEE Transactions on Information Theory*, 58(5):3235–3249, 2012.
- Sungjin Ahn, Anoop Korattikara, and Max Welling. Bayesian posterior sampling via stochastic gradient Fisher scoring. In *Proceedings of the 29th International Conference on Machine Learning*, pages 1771–1778, 2012.
- Shun-ichi Amari. Natural gradient works efficiently in learning. *Neural Computation*, 10(2):251–276, 1998.
- Herman Chernoff. Sequential design of experiments. *The Annals of Mathematical Statistics*, 30(3):755–770, 1959.
- Aryeh Dvoretzky. On stochastic approximation. *Proceedings of the Third Berkeley Symposium on Mathematical Statistics and Probability*, 1:39–55, 1956.
- Stewart N. Ethier and Thomas G. Kurtz. *Markov Processes: Characterization and Convergence*. John Wiley & Sons, 1986.

- Michael C. Fu. Gradient estimation. In Shane G. Henderson and Barry L. Nelson, editors, *Handbooks in Operations Research and Management Science*, volume 13, pages 575–616. Elsevier, 2006.
- Richard D. Gill and Boris Y. Levit. Applications of the Van Trees inequality: A Bayesian Cramér–Rao bound. *Bernoulli*, 1(1/2):59–79, 1995.
- J. Michael Harrison. *Brownian Motion and Stochastic Flow Systems*. John Wiley & Sons, 1985.
- Edwin Hewitt and Leonard J. Savage. Symmetric measures on Cartesian products. *Transactions of the American Mathematical Society*, 80(2):470–501, 1955.
- Nitish Shirish Keskar, Dheevatsa Mudigere, Jorge Nocedal, Mikhail Smelyanskiy, and Ping Tak Peter Tang. On large-batch training for deep learning: Generalization gap and sharp minima. In *International Conference on Learning Representations*, 2017.
- Harold J. Kushner and George G. Yin. *Stochastic Approximation and Recursive Algorithms and Applications*. Springer, 2nd edition, 2003.
- Lucien Le Cam. *Asymptotic Methods in Statistical Decision Theory*. Springer, 1986.
- Erich L. Lehmann and George Casella. *Theory of Point Estimation*. Springer, 2nd edition, 1998.
- Qianxiao Li, Cheng Tai, and Weinan E. Stochastic modified equations and adaptive stochastic gradient algorithms. In *Proceedings of the 34th International Conference on Machine Learning*, pages 2101–2110, 2017.
- Stephan Mandt, Matthew D. Hoffman, and David M. Blei. Stochastic gradient descent as approximate Bayesian inference. *Journal of Machine Learning Research*, 18(1):4873–4907, 2017.
- James Martens. New insights and perspectives on the natural gradient method. *Journal of Machine Learning Research*, 21(146):1–76, 2020.
- James Martens and Roger Grosse. Optimizing neural networks with Kronecker-factored approximate curvature. In *Proceedings of the 32nd International Conference on Machine Learning*, pages 2408–2417, 2015.
- Sam McCandlish, Jared Kaplan, Dario Amodei, and OpenAI Dota Team. An empirical model of large-batch training. *arXiv preprint arXiv:1812.06162*, 2018.
- Arkadi Nemirovski, Anatoli Juditsky, Guanghui Lan, and Alexander Shapiro. Robust stochastic approximation approach to stochastic programming. *SIAM Journal on Optimization*, 19(4):1574–1609, 2009.

- Yurii Nesterov. *Introductory Lectures on Convex Optimization: A Basic Course*. Kluwer Academic Publishers, 2004.
- Courtney Paquette, Elliot Paquette, Ben Adlam, and Jeffrey Pennington. Homogenization of SGD in high-dimensions: Exact dynamics and generalization properties. *Mathematical Programming*, 214:1–90, 2025. doi: 10.1007/s10107-024-02171-3.
- Boris T. Polyak and Anatoli B. Juditsky. Acceleration of stochastic approximation by averaging. *SIAM Journal on Control and Optimization*, 30(4):838–855, 1992.
- Herbert Robbins and Sutton Monro. A stochastic approximation method. *The Annals of Mathematical Statistics*, 22(3):400–407, 1951.
- Christopher J Shallue, Jaehoon Lee, Joseph Antognini, Jascha Sohl-Dickstein, Roy Frostig, and George E Dahl. Measuring the effects of data parallelism on neural network training. *Journal of Machine Learning Research*, 20(112):1–49, 2019.
- Alexander Shapiro, Darinka Dentcheva, and Andrzej Ruszczyński. *Lectures on Stochastic Programming: Modeling and Theory*. SIAM, 2nd edition, 2014.
- Samuel L Smith, Benoit Dherin, David GT Barrett, and Soham De. On the origin of implicit regularization in stochastic gradient descent. *International Conference on Learning Representations*, 2021.
- Joel A. Tropp. *An Introduction to Matrix Concentration Inequalities*. Foundations and Trends in Machine Learning, 2015.
- A. W. van der Vaart. *Asymptotic Statistics*. Cambridge University Press, 1998.
- Roman Vershynin. *High-Dimensional Probability: An Introduction with Applications in Data Science*. Cambridge University Press, 2018.
- Martin J. Wainwright. *High-Dimensional Statistics: A Non-Asymptotic Viewpoint*. Cambridge Series in Statistical and Probabilistic Mathematics. Cambridge University Press, 2019.
- Ward Whitt. *Stochastic-Process Limits: An Introduction to Stochastic-Process Limits and Their Application to Queues*. Springer, 2002.